ICES REPORT 11-09

April 2011

Analysis of an Hp-Non-conforming Discontinuous Galerkin Spectral Element Method for Wave

by

Tan Bui-Thanh and Omar Ghattas

The Institute for Computational Engineering and Sciences
The University of Texas at Austin
Austin, Texas 78712

Reference: Tan Bui-Thanh and Omar Ghattas, "Analysis of an Hp-Non-conforming Discontinuous Galerkin Spectral Element Method for Wave Propagation", ICES REPORT 11-09, The Institute for Computational Engineering and Sciences, The University of Texas at Austin, April 2011.

Report Documentation Page

Form Approved
OMB No. 0704-0188

1. REPORT DATE	2. REPORT TYPE	3. DATES COVERED
APR 2011		**00-00-2011 to 00-00-2011**

4. TITLE AND SUBTITLE	5a. CONTRACT NUMBER
Analysis of an Hp-Non-conforming Discontinuous Galerkin Spectral Element Method for Wave	5b. GRANT NUMBER
	5c. PROGRAM ELEMENT NUMBER
6. AUTHOR(S)	5d. PROJECT NUMBER
	5e. TASK NUMBER
	5f. WORK UNIT NUMBER
7. PERFORMING ORGANIZATION NAME(S) AND ADDRESS(ES) **University of Texas at Austin,Institute for Computational Engineering and Sciences,Austin,TX,78712**	8. PERFORMING ORGANIZATION REPORT NUMBER
9. SPONSORING/MONITORING AGENCY NAME(S) AND ADDRESS(ES)	10. SPONSOR/MONITOR'S ACRONYM(S)
	11. SPONSOR/MONITOR'S REPORT NUMBER(S)

12. DISTRIBUTION/AVAILABILITY STATEMENT
Approved for public release; distribution unlimited

13. SUPPLEMENTARY NOTES

14. ABSTRACT

We analyze the consistency, stability, and convergence of an hp discontinuous Galerkin spectral element method. The analysis is carried out simultaneously for acoustic, elastic coupled elastic{acoustic, and electromagnetic wave propagation. Our analytical results are developed for both conforming and non-conforming approximations on hexahedral meshes using either exact integration with Legendre-Gauss quadrature or inexact integration with Legendre-Gauss-Lobatto quadrature. A mortar-based non-conforming approximation is developed to treat both h and p non-conforming meshes simultaneously. The mortar approach is constructed in such a way that consistency, stability, and convergence analyses for non-conforming approximations follows the con- forming counterparts with minimal modi cations. In particular, sharp hp-convergence results are proved for non-conforming approximations for time dependent wave propagation problems using inexact quadrature.

15. SUBJECT TERMS

16. SECURITY CLASSIFICATION OF:			17. LIMITATION OF ABSTRACT	18. NUMBER OF PAGES	19a. NAME OF RESPONSIBLE PERSON
a. REPORT **unclassified**	b. ABSTRACT **unclassified**	c. THIS PAGE **unclassified**	**Same as Report (SAR)**	**25**	

ANALYSIS OF AN HP-NON-CONFORMING DISCONTINUOUS GALERKIN SPECTRAL ELEMENT METHOD FOR WAVE PROPAGATION*

TAN BUI-THANH † AND OMAR GHATTAS †‡§

Abstract. We analyze the consistency, stability, and convergence of an hp discontinuous Galerkin spectral element method. The analysis is carried out simultaneously for acoustic, elastic, coupled elastic–acoustic, and electromagnetic wave propagation. Our analytical results are developed for both conforming and non-conforming approximations on hexahedral meshes using either exact integration with Legendre-Gauss quadrature or inexact integration with Legendre-Gauss-Lobatto quadrature. A mortar-based non-conforming approximation is developed to treat both h and p non-conforming meshes simultaneously. The mortar approach is constructed in such a way that consistency, stability, and convergence analyses for non-conforming approximations follows the conforming counterparts with minimal modifications. In particular, sharp hp-convergence results are proved for non-conforming approximations for time dependent wave propagation problems using inexact quadrature.

Key words. discontinuous Galerkin method; spectral element method; linear hyperbolic equations; acoustic, elastic, and electromagnetic wave propagation; Riemann flux; non-conforming meshes; Legendre-Gauss; Legendre-Gauss-Lobatto; consistency, stability, convergence.

AMS subject classifications. 65N35, 65N12, 65N15

1. Introduction.

The discontinuous Galerkin (DG) method was originally developed by Reed and Hill [21] for the neutron transport equation, but has been extended to other problems governed by partial differential equations (PDEs) [9]. In particular, it has emerged as a particularly attractive method for hyperbolic PDEs [8, 10]. Among its many advantages over classical finite volume and finite element methods, it has the ability to treat solutions with large gradients including shocks, it provides the flexibility to deal with complex geometries, and it is highly parallelizable due to its compact stencil. Perhaps its most important advantage, however, is its ability to support hp adaptivity (where h refers to mesh size, and p to local polynomial order) in a natural manner [5]. Together, these advantages make DG a very desirable method for parallel solution of large-scale hyperbolic problems on adapted meshes (e.g., [27]).

The question of how to treat non-conforming interfaces between elements due to both local p-refinement and local h-refinement can be addressed in several ways. The non-conforming approach of Kopriva [14, 18] replaces a non-conforming face by mortars that connect pairs of contributing elements. The actual computations are performed on the mortars instead of the non-conforming faces, and the results are then projected onto the contributing element faces. Since the mortar approach maintains the compact stencil of the DG method, it makes adaptivity highly parallelizable [27]. Moreover, discrete stability and optimal convergence rates have been numerically observed in practice [18, 27]. Since then, there have been no attempts to theoretically

†Institute for Computational Engineering & Sciences, The University of Texas at Austin, Austin, TX 78712, USA.

‡Jackson School of Geosciences, The University of Texas at Austin, Austin, TX 78712, USA.

§Department of Mechanical Engineering, The University of Texas at Austin, Austin, TX 78712, USA.

*This work was supported by AFOSR grant FA9550-09-1-0608 and NSF grants CDI-1028889 and DMS-0724746.

study the stability and convergence of Kopriva's mortar-based non-conforming approximation in the context of discontinuous Galerkin spectral element methods. This is the subject of the present article.

The celebrated Lax-Richtmyer equivalence theorem [20] has far reaching consequences in numerical analysis, so much so that it is sometimes called the fundamental theorem of numerical analysis. The theorem says that for well-posed linear differential problems, consistency and stability of a difference method imply its convergence. However, typical applications of the Lax-Richtmyer theorem provide an upper bound on error that grows exponentially in time. In practice, it is observed that the error grows at a much lower rate. Rather than rely on the equivalence theorem, it has been shown that a direct proof of convergence, with an error bound that grows at most linearly in time, is possible for a class of discontinuous Galerkin methods [12, 13].

In this paper, we study theoretically the consistency, stability, and convergence of a discontinuous Galerkin spectral element method (DGSEM) using such a direct proof. In particular, we present a stability proof using an energy method for the DGSEM with the mortar-based non-conforming approximation of Kopriva [14, 18]. We expect that the results of our study can be applied to a large class of linear conservation laws. However, for concreteness, the proof is simultaneously carried out for elastic, acoustic, coupled elastic–acoustic, and electromagnetic wave equations, as exemplary conservation laws governed by linear hyperbolic PDEs. Instead of using an exact numerical quadrature for the mortars as in [18, 27], for which we are not able to prove stability in the interesting case of Legendre-Gauss-Lobatto quadrature, we propose to employ a particular kind of quadrature rule that not only facilitates the stability proof, but is also cheaper.

We are able to prove stability and convergence for both exact numerical quadrature using the Legendre-Gauss rule and inexact numerical quadrature using the Legendre-Gauss-Lobatto rule. For the inexact numerical integration, we use the tensor product quadrature rule, since it allows us to perform discrete integration by parts [24, 17], which in turns paves the way for the stability and convergence proofs.

The Riemann numerical flux is our main ingredient in proving stability and convergence. Since the PDEs in this paper are linear, the exact Riemann flux can be derived [25], and therefore we use it in our proofs. As will be shown, it is the dissipative nature of the Riemann flux that makes the DGSEM stable. Therefore, we speculate that our results also hold for other dissipative fluxes such as the stabilized Lax-Friedrichs numerical flux [22].

We mostly restrict ourselves to the case of affine hexahedral meshes, for which details of the derivations and proofs are presented. In order to make the proofs concrete, three-dimensional coupled elastic–acoustic and electromagnetic waves are used as examples. Of course, all of the results hold for two-dimensional problems as well.

This article is organized as follows. Section §2 briefly describes a weak setting for general linear conservation laws. Section §3 presents an *hp* DGSEM for both elastic–acoustic and electromagnetic waves. We then prove stability for conforming meshes in §4. The detailed description of our mortar-based non-conforming approximation is given in §5, which is followed by the non-conforming stability proof in §6. The direct proof of convergence is carried out in §7, and Section §8 offers conclusions.

2. General setting for linear hyperbolic conservation laws. We are interested in linear wave equations governed by linear hyperbolic conservation laws. In

the strong form, a general equation is given as

$$\mathcal{Q}\frac{\partial \mathfrak{q}}{\partial t} + \nabla_{\boldsymbol{x}} \cdot (\mathfrak{F}\mathfrak{q}) = \mathfrak{g}, \quad \mathfrak{q} \in \mathcal{V}, \boldsymbol{x} \in \mathcal{D},$$

with $\mathcal{V}$ as the solution space, to be specified later, over the domain of interest $\mathcal{D}$, and with appropriate initial and boundary conditions. The subscript $\boldsymbol{x}$ denotes the $\boldsymbol{x}$-coordinate system in which the divergence operator acts. Next, multiplying by the test function $\mathfrak{p}$, the corresponding weak formulation is obtained as

$$\int_{\mathcal{D}} \mathcal{Q}\frac{\partial \mathfrak{q}}{\partial t} \cdot \mathfrak{p}\, d\boldsymbol{x} + \int_{\mathcal{D}} \nabla_{\boldsymbol{x}} \cdot (\mathfrak{F}\mathfrak{q}) \cdot \mathfrak{p}\, d\boldsymbol{x} = \int_{\mathcal{D}} \mathfrak{g} \cdot \mathfrak{p}\, d\boldsymbol{x},$$

where "$\cdot$" denotes the Euclidean inner product.

We next partition the domain $\mathcal{D}$ into N_{el} non-overlapping hexahedral elements such that $\mathcal{D} = \bigcup_{e=1}^{N_{\text{el}}} \mathsf{D}^e$, and integrate the weak formulation by parts twice to obtain

$$\begin{aligned}&\sum_e \int_{\mathsf{D}^e} \mathcal{Q}^e \frac{\partial \mathfrak{q}^e}{\partial t} \cdot \mathfrak{p}^e\, d\boldsymbol{x} + \int_{\mathsf{D}^e} \nabla_{\boldsymbol{x}} \cdot (\mathfrak{F}\mathfrak{q}^e) \cdot \mathfrak{p}^e\, d\boldsymbol{x} \\ &+ \int_{\partial \mathsf{D}^e} \boldsymbol{n} \cdot \left[(\mathfrak{F}\mathfrak{q}^e)^* - \mathfrak{F}\mathfrak{q}^e\right] \cdot \mathfrak{p}^e\, d\boldsymbol{x} = \sum_e \int_{\mathsf{D}^e} \mathfrak{g}^e \cdot \mathfrak{p}^e\, d\boldsymbol{x}, \end{aligned} \tag{2.1}$$

where a consistent numerical flux $(\mathfrak{F}\mathfrak{q}^e)^*$ has been introduced to couple solutions of neighboring elements, and $(\cdot)^e$ denotes the restriction on the e-th element of the corresponding quantity.

Equation (2.1) is known as the strong form in the context of nodal discontinuous Galerkin methods [13]. For the DGSEM described in this paper, the strong form (integrating the flux terms by parts twice) and the weak form (integrating the flux terms by parts once) are equivalent [24, 17], and hence all the results in the paper hold for the weak form as well.

3. A discontinuous Galerkin spectral element method. In this section, we briefly describe an *hp*-discontinuous Galerkin spectral element method. We approximate each element D^e by polynomials, again denoted by D^e, such that each element D^e is mapped to the reference hexahedron $\hat{\mathsf{D}} = [-1, 1]^3$ by a C^1-diffeomorphism $\boldsymbol{X}^e$, and $\mathcal{D} \approx \mathcal{D}^{N_{el}} = \bigcup_{e=1}^{N_{el}} \mathsf{D}^e$. Equation (2.1) can be written in terms of $\hat{\mathsf{D}}$ as

$$\begin{aligned}&\sum_e \int_{\hat{\mathsf{D}}} J^e \mathcal{Q}^e \frac{\partial \mathfrak{q}^e}{\partial t} \cdot \mathfrak{p}^e\, d\boldsymbol{r} + \int_{\hat{\mathsf{D}}} \nabla_{\boldsymbol{r}} \cdot \left(\tilde{\mathfrak{F}}\mathfrak{q}^e\right) \cdot \mathfrak{p}^e\, d\boldsymbol{r} \\ &+ \int_{\partial \hat{\mathsf{D}}} \tilde{\boldsymbol{n}} \cdot \left[\left(\tilde{\mathfrak{F}}\mathfrak{q}^e\right)^* - \tilde{\mathfrak{F}}\mathfrak{q}^e\right] \cdot \mathfrak{p}^e\, d\boldsymbol{r} = \sum_e \int_{\hat{\mathsf{D}}} J^e \mathfrak{g}^e \cdot \mathfrak{p}^e\, d\boldsymbol{r}, \end{aligned} \tag{3.1}$$

where $\boldsymbol{r} = (r_1, r_2, r_3) \in \hat{\mathsf{D}}$ represents the reference coordinates and J^e is the Jacobian of the transformation. The outward normal on the boundary of the master element $\hat{\mathsf{D}}$ is denoted by $\tilde{\boldsymbol{n}}$, and the contravariant flux [15] is defined as

$$\tilde{\mathfrak{F}}^i = J^e \boldsymbol{a}^i \cdot \mathfrak{F}, \quad i = 1, 2, 3,$$

with $\boldsymbol{a}^i$ as the contravariant basis vectors.

We now describe the approximation spaces for wave propagation in elastic, acoustic, and coupled elastic–acoustic media using the strain–velocity formulation, and for

Maxwell's equations for electromagnetic wave propagation. Equation (3.1) can be specialized to the elastic–acoustic wave propagation case by the following definitions,

$$\mathfrak{q} = \begin{pmatrix} \boldsymbol{E} \\ \boldsymbol{v} \end{pmatrix} \in \mathcal{V}, \quad \mathcal{Q} = \begin{pmatrix} \mathsf{I} & \mathbf{0} \\ \mathbf{0} & \rho \boldsymbol{I} \end{pmatrix}, \quad \mathfrak{g} = \begin{pmatrix} \mathbf{0} \\ \boldsymbol{f} \end{pmatrix} \in \mathcal{V},$$

with I denoting the fourth-order identity tensor, $\mathbf{0}$ the zero tensors of appropriate sizes, $\boldsymbol{I}$ the second-order identity tensor, $\boldsymbol{E}$ the strain tensor, $\boldsymbol{v}$ the velocity vector, $\boldsymbol{f}$ the external volumetric forces, and ρ the density.

The action of the flux operator $\mathfrak{F}$ on the strain–velocity unknowns $\mathfrak{q}$ can be shown to be [27]

$$(\mathfrak{F}\mathfrak{q})_i = \begin{pmatrix} -\frac{1}{2}\left(\boldsymbol{v} \otimes \boldsymbol{e}_i + \boldsymbol{e}_i \otimes \boldsymbol{v}\right) \\ -\left(\mathsf{C}\boldsymbol{E}\right)\boldsymbol{e}_i \end{pmatrix} \in \mathcal{V}, \quad \text{for } i = 1, 2, 3.$$

For isotropic linear elasticity, the strain tensor $\boldsymbol{E}$ and the Cauchy stress tensor $\boldsymbol{S}$ are related by the fourth-order constitutive tensor C,

$$\boldsymbol{S} = \mathsf{C}\boldsymbol{E} = \lambda \operatorname{tr}(\boldsymbol{E})\boldsymbol{I} + 2\mu\boldsymbol{E},$$

where λ and μ are the two Lamé constants characterizing the isotropic constitutive relationship. The longitudinal wave speed c_p and shear wave speed c_s are defined in terms of the Lamé constants and density by

$$c_p = \sqrt{\frac{\lambda + 2\mu}{\rho}} \qquad \text{and} \qquad c_s = \sqrt{\frac{\mu}{\rho}},$$

with $c_s = 0$ in acoustic regions by virtue of $\mu = 0$.

As in [27], we choose the solution space to be $\mathcal{V} = \boldsymbol{V}_{\text{sym}}^{3\times 3} \oplus \boldsymbol{V}^3$, where $\boldsymbol{V}$ denotes a space of sufficiently smooth functions defined on $\mathcal{D}$ so that (2.1) makes sense. The discontinuous approximation to $\boldsymbol{V}$ is given by

$$\boldsymbol{V}_d := \{q_d \in L^2(\mathcal{D}^{N_{\text{el}}}) : q_d|_{\mathsf{D}^e} \circ \boldsymbol{X}^e \in \mathbb{Q}_{N_e}(\hat{\mathsf{D}})\},$$

where $\mathbb{Q}_{N_e}$ is the tensor product of one-dimensional polynomials of degree at most N_e on the reference element. It should be pointed out that the polynomial orders need not be the same for all directions. Nevertheless, we use the same order for clarity of the exposition. The numerical solution $\mathfrak{q}_d \in \boldsymbol{V}_{d,\text{sym}}^{3\times 3} \oplus \boldsymbol{V}_d^3$ restricted on each element D^e is specified as

$$\mathfrak{q}_d|_{\mathsf{D}^e} \circ \boldsymbol{X}^e \in \mathcal{V}_d^e \equiv \mathbb{Q}_{N_e,\text{sym}}^{3\times 3} \oplus \mathbb{Q}_{N_e}^3, \qquad \boldsymbol{X}^e : \hat{\mathsf{D}} \to \mathsf{D}^e.$$

Before introducing the Riemann flux, let us recall the following standard DG notation for quantities associated with element interfaces:

$$[\![\mathfrak{q}]\!] = \mathfrak{q}^+ \cdot \boldsymbol{n}^+ + \mathfrak{q}^- \cdot \boldsymbol{n}^-, \quad [\mathfrak{q}] = \mathfrak{q}^- - \mathfrak{q}^+, \quad \{\{Z\}\} = \frac{Z^+ + Z^-}{2},$$

where the positive and negative signs indicate element interior and exterior, respectively.

For linear conservation laws one can solve the Riemann problem exactly by various methods [25]. Using the Rankine–Hugoniot approach, Wilcox *et al.* [27] show that

the exact Riemann flux for the strain equation is given by

$$\begin{aligned}\boldsymbol{n}\cdot\left[(\mathfrak{F}\mathfrak{q})^*_{\boldsymbol{E}}-(\mathfrak{F}\mathfrak{q})_{\boldsymbol{E}}\right]=&\left(k_0\boldsymbol{n}\cdot[\![\mathbf{C}\boldsymbol{E}]\!]+k_0\rho^+c_p^+[\![\boldsymbol{v}]\!]\right)\boldsymbol{n}\otimes\boldsymbol{n}\\&-k_1\,\mathrm{sym}\left(\boldsymbol{n}\otimes(\boldsymbol{n}\times(\boldsymbol{n}\times[\![\mathbf{C}\boldsymbol{E}]\!]))\right)\\&-k_1\rho^+c_s^+\,\mathrm{sym}\left(\boldsymbol{n}\otimes(\boldsymbol{n}\times(\boldsymbol{n}\times[\boldsymbol{v}]))\right),\end{aligned}$$

and for the velocity equation by

$$\begin{aligned}\boldsymbol{n}\cdot\left[(\mathfrak{F}\mathfrak{q})^*_{\boldsymbol{v}}-(\mathfrak{F}\mathfrak{q})_{\boldsymbol{v}}\right]=&\left(k_0\boldsymbol{n}\cdot[\![\mathbf{C}\boldsymbol{E}]\!]+k_0\rho^+c_p^+[\![\boldsymbol{v}]\!]\right)\rho^-c_p^-\boldsymbol{n}\\&-k_1\rho^-c_s^-\boldsymbol{n}\times(\boldsymbol{n}\times[\![\mathbf{C}\boldsymbol{E}]\!])\\&-k_1\rho^+c_s^+\rho^-c_s^-\boldsymbol{n}\times(\boldsymbol{n}\times[\boldsymbol{v}]),\end{aligned}$$

with $k_0=\left(\rho^-c_p^-+\rho^+c_p^+\right)^{-1}$, $k_1=\left(\rho^-c_s^-+\rho^+c_s^+\right)^{-1}$ if $\mu^-\neq 0$, and $k_1=0$ if $\mu^-=0$. Here, we will consider only traction boundary conditions $\boldsymbol{S}\boldsymbol{n}=\boldsymbol{t}_{bc}$, where $\boldsymbol{t}_{bc}$ is the prescribed traction. The traction condition is enforced by the following mirror principle,

$$[\![\boldsymbol{v}]\!]=[\boldsymbol{v}]=\mathbf{0},\quad\text{and}\quad[\![\boldsymbol{S}]\!]=-2\left(\boldsymbol{t}_{bc}-\boldsymbol{S}^-\boldsymbol{n}\right),$$

which applies to both elastic and acoustic media.

We next specialize (3.1) to the case of Maxwell's equations. In this case,

$$\mathfrak{q}=\begin{pmatrix}\boldsymbol{E}\\\boldsymbol{H}\end{pmatrix}\in\mathcal{V},\quad\mathcal{Q}=\begin{pmatrix}\varepsilon\boldsymbol{I}&\mathbf{0}\\\mathbf{0}&\mu\boldsymbol{I}\end{pmatrix},\quad\mathfrak{g}=\begin{pmatrix}\mathbf{0}\\\mathbf{0}\end{pmatrix}\in\mathcal{V},$$

where $\boldsymbol{E}$ denotes the electric field, $\boldsymbol{H}$ the magnetic field, μ the permeability, and ε the permittivity.

The action of the flux operator $\mathfrak{F}$ on the electromagnetic field $\mathfrak{q}$ is defined by

$$(\mathfrak{F}\mathfrak{q})_i=\begin{pmatrix}-\boldsymbol{e}_i\times\boldsymbol{H}\\\boldsymbol{e}_i\times\boldsymbol{E}\end{pmatrix}\in\mathcal{V},\quad\text{for } i=1,2,3,$$

where $\mathcal{V}=\boldsymbol{V}^3$ and $\mathfrak{q}_d|_{\mathsf{D}^e}\circ\boldsymbol{X}^e\in\mathcal{V}_d^e\equiv\mathbb{Q}_{N_e}^3$. The exact Riemann numerical flux for electric equation can be shown to be [13]

$$\boldsymbol{n}\cdot\left[(\mathfrak{F}\mathfrak{q})^*_{\boldsymbol{E}}-(\mathfrak{F}\mathfrak{q})_{\boldsymbol{E}}\right]=\frac{1}{2\,\{\{Z\}\}}\boldsymbol{n}\times\left(Z^+[\boldsymbol{H}]-\boldsymbol{n}\times[\boldsymbol{E}]\right),$$

and for the magnetic equation,

$$\boldsymbol{n}\cdot\left[(\mathfrak{F}\mathfrak{q})^*_{\boldsymbol{H}}-(\mathfrak{F}\mathfrak{q})_{\boldsymbol{H}}\right]=-\frac{1}{2\,\{\{Y\}\}}\boldsymbol{n}\times\left(Y^+[\boldsymbol{E}]+\boldsymbol{n}\times[\boldsymbol{H}]\right),$$

where

$$Z^\pm=\frac{1}{Y^\pm}=\sqrt{\frac{\mu^\pm}{\epsilon^\pm}}.$$

Similar to the elastic–acoustic coupling case, we use the mirror principle to enforce a perfect electric conductor (PEC) boundary condition by

$$Z^-=Z^+,\quad Y^-=Y^+,\quad\boldsymbol{n}\times[\boldsymbol{H}]=0,\quad\boldsymbol{n}\times[\boldsymbol{E}]=2\boldsymbol{n}\times\boldsymbol{E}^-,$$

and a perfect magnetic conductor (PMC) boundary condition by

$$Z^- = Z^+, \quad Y^- = Y^+, \quad \boldsymbol{n} \times [\boldsymbol{E}] = 0, \quad \boldsymbol{n} \times [\boldsymbol{H}] = 2\boldsymbol{n} \times \boldsymbol{H}^-.$$

For dielectric boundary conditions we use

$$\boldsymbol{n} \times \boldsymbol{E}^- = \boldsymbol{n} \times \boldsymbol{E}^+, \quad \boldsymbol{n} \times \boldsymbol{H}^- = \boldsymbol{n} \times \boldsymbol{H}^+.$$

In order to unify the treatment for elastic, acoustic, coupled elastic–acoustic, and electromagnetic waves, we define a generic polynomial space $\mathcal{P}_N$ whose meaning will be clear in each context. For example, if we write $\mathfrak{q}^e \in \mathcal{P}_N$, this identifies $\mathcal{P}_N \equiv \mathcal{V}_d^e$.

The tensor product basis for $\mathbb{Q}_N$ is built upon the following one-dimensional Lagrange basis

$$\ell_l(\xi) = \prod_{\substack{k=0,1,\ldots,N \\ k \neq l}} \frac{\xi - \xi_k}{\xi_l - \xi_k},$$

where the Nth-degree Legendre-Gauss-Lobatto (LGL) points, or Nth-degree Legendre-Gauss points (LG), $\{\xi_l\}$ on $[-1, 1]$ for $l = 0, \ldots, N$, are chosen as both the interpolation and quadrature points. This is also known as the collocation approach. The Lagrange interpolant of a function $f(\boldsymbol{r})$ on the reference element $\hat{\mathsf{D}}$ is defined through the interpolation operator $\mathcal{I}_N$ as

$$\mathcal{I}_N(f) = \sum_{l,m,n=0}^{N} f_{lmn} \ell_l(r_1) \ell_m(r_2) \ell_n(r_3), \quad f_{lmn} = f(\boldsymbol{\xi}_{lmn}), \quad \boldsymbol{\xi}_{lmn} = (\xi_l, \xi_m, \xi_n) \in \hat{\mathsf{D}}.$$

A typical collocation approach [16] in semi-discretizing (3.1) is as follows. Find $\mathfrak{q} \in \mathcal{V}_d$ such that

$$\begin{aligned}
&\sum_e \int_{\hat{\mathsf{D}}, N_e} \mathcal{I}_{N_e} \left(\mathcal{I}_{N_e}(J^e) \mathcal{I}_{N_e}(\mathcal{Q}^e) \frac{\partial \mathfrak{q}^e}{\partial t} \right) \cdot \mathfrak{p}^e \, d\boldsymbol{r} + \int_{\hat{\mathsf{D}}, N_e} \nabla_{\boldsymbol{r}} \cdot \mathcal{I}_{N_e} \left(\tilde{\mathfrak{F}} \mathfrak{q}^e \right) \cdot \mathfrak{p}^e \, d\boldsymbol{r} \\
&+ \int_{\partial \hat{\mathsf{D}}, N_e} \tilde{\boldsymbol{n}} \cdot \left[\mathcal{I}_{N_e} \left(\left(\tilde{\mathfrak{F}} \mathfrak{q}^e \right)^* \right) - \mathcal{I}_{N_e} \left(\tilde{\mathfrak{F}} \mathfrak{q}^e \right) \right] \cdot \mathfrak{p}^e \, d\boldsymbol{r} \\
&= \sum_e \int_{\hat{\mathsf{D}}, N_e} \mathcal{I}_{N_e} \left(\mathcal{I}_{N_e}(J^e) \mathcal{I}_{N_e}(\mathfrak{g}^e) \right) \cdot \mathfrak{p}^e \, d\boldsymbol{r}, \quad \forall \mathfrak{p} \in \mathcal{V}_d,
\end{aligned} \tag{3.2}$$

where $\mathcal{I}_{N_e} \left(\tilde{\mathfrak{F}}^i \right) = \mathcal{I}_{N_e} \left(\mathcal{I}_{N_e} \left(J^e \boldsymbol{a}^i \right) \cdot \mathcal{I}_{N_e} (\mathfrak{F}) \right)$. The direct consequence of the above collocation is that the integrand in each integral is at most of order $2N_e$ in each direction $r_i, i = 1, 2, 3$. The subscript N_e in the integrals means that the integrals are numerically evaluated using the corresponding N_eth-degree LGL (or LG) quadrature rule.

4. Semi-discrete stability for conforming meshes. In this section, we provide a stability proof for the both elastic–acoustic and electromagnetic cases on conforming meshes. By conforming meshes we mean that the intersection of two elements is either an entire face, and entire edge, or a corner, and that the solution order is the same for all elements. It is sufficient to prove semi-discrete stability since, by a result in [19] (and the references therein), if the semi-discrete equation is stable, the fully discrete system with the time derivative discretized by a locally stable Runge-Kutta

(for example the classical 4th-order Runge-Kutta method) is stable as well, as long as the time step is sufficiently small.

Here, we employ the energy approach to prove stability. For the elastic–acoustic case, the semi-discrete energy functional $\mathcal{E}_d(t)$ is defined as

$$\mathcal{E}_d(t) := \sum_{e=1}^{N_{\text{el}}} \mathcal{E}^e_{N^e}(t) \quad \text{where} \quad \mathcal{E}^e_{N^e}(t) := \frac{1}{2}\int_{\mathsf{D}^e,N_e} (\boldsymbol{E} : (\mathbf{C}\boldsymbol{E}) + \rho \boldsymbol{v}\cdot\boldsymbol{v})\, d\boldsymbol{x},$$

and for the electromagnetic case as

$$\mathcal{E}_d(t) := \sum_{e=1}^{N_{\text{el}}} \mathcal{E}^e_{N^e}(t) \quad \text{where} \quad \mathcal{E}^e_{N^e}(t) := \frac{1}{2}\int_{\mathsf{D}^e,N_e} (\epsilon \boldsymbol{E}\cdot\boldsymbol{E} + \mu \boldsymbol{H}\cdot\boldsymbol{H})\, d\boldsymbol{x}.$$

For convenience, we define the element-wise discrete L^2 inner product and the induced norm on a generic domain D, which could be an element or its boundary, as

$$(\mathfrak{q},\mathfrak{p})_{D,N} = \int_{D,N} \mathfrak{q}\cdot\mathfrak{p}\, d\boldsymbol{x}, \quad \|\mathfrak{q}\|^2_{D,N} = \int_{D,N} \mathfrak{q}\cdot\mathfrak{q}\, d\boldsymbol{x},$$

and their continuous counterparts as

$$(\mathfrak{q},\mathfrak{p})_{D} = \int_{D} \mathfrak{q}\cdot\mathfrak{p}\, d\boldsymbol{x}, \quad \|\mathfrak{q}\|^2_{D} = \int_{D} \mathfrak{q}\cdot\mathfrak{p}\, d\boldsymbol{x}.$$

The discrete global L^2 norm is computed as the summation of the element-wise contributions

$$\|\mathfrak{q}\|^2_{\mathcal{D}^{N_{\text{el}}},d} = \sum_e \|\mathfrak{q}\|^2_{\mathsf{D}^e,N^e}.$$

THEOREM 1 (Stability for conforming meshes). *Assume the mesh is affine and conforming with solution order N, then the DGSEM discretization is stable in the following sense:*

$$\frac{d}{dt}\mathcal{E}_d \le \frac{1}{2}\left(\mathcal{E}_d + \|\mathcal{I}_N\mathfrak{g}\|^2_{\mathcal{D}^{N_{el}},d}\right).$$

Moreover, if $\mathfrak{g}=0$, then $\frac{d}{dt}\mathcal{E}_d \le 0$.

Proof. Substituting $\mathfrak{p} := \begin{pmatrix}\boldsymbol{S}\\ \boldsymbol{v}\end{pmatrix} := \begin{pmatrix}\mathbf{C}\boldsymbol{E}\\ \boldsymbol{v}\end{pmatrix}$ for the elastic–acoustic coupling case, and $\mathfrak{p}=\mathfrak{q}$ for the electromagnetic case, into (3.2), and using a discrete integration by parts formula [24, 17], we obtain

$$\begin{aligned}\sum_e \frac{d}{dt}\mathcal{E}^e_d = \frac{1}{2}\sum_e \int_{\hat{\mathsf{D}},N} \left[\mathcal{I}_N\left(\tilde{\mathfrak{F}}\mathfrak{q}^e\right)\cdot\nabla_{\boldsymbol{r}}\cdot\mathfrak{p}^e - \nabla_{\boldsymbol{r}}\cdot\mathcal{I}_N\left(\tilde{\mathfrak{F}}\mathfrak{q}^e\right)\cdot\mathfrak{p}^e\right] d\boldsymbol{r}\\ - \int_{\partial\hat{\mathsf{D}},N} \tilde{\boldsymbol{n}}\cdot\left[\left(\tilde{\mathfrak{F}}\mathfrak{q}^e\right)^* - \frac{1}{2}\tilde{\mathfrak{F}}\mathfrak{q}^e\right]\cdot\mathfrak{p}^e\, d\boldsymbol{r} + \int_{\hat{\mathsf{D}},N} J^e\mathfrak{g}^e\cdot\mathfrak{p}^e\, d\boldsymbol{r}, \quad (4.1)\end{aligned}$$

where we have dropped the interpolation operator $\mathcal{I}_{N_e}$ in the last two terms on the right side of (4.1) since the interpolation is an orthogonal projection with the discrete L^2 inner product [7], e.g.,

$$\int_{D,N} qp\, d\boldsymbol{x} = \int_{D,N} \mathcal{I}_N(q)\, p\, d\boldsymbol{x}. \quad (4.2)$$

For affine meshes, the metric terms $J^e\boldsymbol{a}^i, i = 1, 2, 3$ are constant, and thus

$$\mathcal{I}_N\left(\tilde{\mathfrak{F}}^i\right) = J^e\boldsymbol{a}^i \cdot \mathcal{I}_N\left(\mathfrak{F}\right).$$

After some simple manipulations, for either the elastic-acoustic case or the electromagnetic case, one has

$$\int_{\hat{\mathsf{D}},N} \left(\mathcal{I}_N\left(\tilde{\mathfrak{F}}\mathfrak{q}^e\right) \cdot \nabla_{\boldsymbol{r}}\mathfrak{p}^e - \nabla_{\boldsymbol{r}} \cdot \mathcal{I}_N\left(\tilde{\mathfrak{F}}\mathfrak{q}^e\right) \cdot \mathfrak{p}^e\right) d\boldsymbol{r} = 0.$$

As a result, the volume terms vanish and the preceding equation can be expressed in the integrals over physical space as

$$\sum_e \frac{d}{dt}\mathcal{E}_d^e \;=\; -\sum_e \int_{\partial\mathsf{D}^e,N} \boldsymbol{n} \cdot \left[(\mathfrak{F}\mathfrak{q}^e)^* - \frac{1}{2}\mathfrak{F}\mathfrak{q}^e\right] \cdot \mathfrak{p}^e\, d\boldsymbol{x} + \int_{\mathsf{D}^e,N} \mathfrak{g}^e \cdot \mathfrak{p}^e\, d\boldsymbol{x}. \quad (4.3)$$

Next, if $\partial\mathsf{D}^e \cap \partial\mathsf{D}^{e'}$ is a non-empty two-dimensional intersection ($\partial\mathsf{D}^e \cap \partial\mathsf{D}^{e'}$ has non-zero two-dimensional Lebesgue measure) we combine the integrands of the surface integrals on both "$-$" and "$+$" LGL (or LG) points. This is possible due to the mesh conformity, i.e., the number of LGL (or LG) points on "$-$" and "$+$" sides are the same and they can be reordered to be exactly coincident. After some algebraic manipulations for the surface integrals on the right side of (4.3), the following holds for the elastic–acoustic case:

$$\begin{aligned}\sum_e \frac{d}{dt}\mathcal{E}_d^e = &-\frac{1}{2}\sum_e \int_{\partial\mathsf{D}^e,N} k_0 \left\{(\boldsymbol{n} \cdot [\![\boldsymbol{S}]\!])^2 + \rho^- c_p^- \rho^+ c_p^+ [\![\boldsymbol{v}]\!]^2\right\} \\ &+ k_1 \left\{\|\boldsymbol{n} \times (\boldsymbol{n} \times [\![\boldsymbol{S}]\!])\|^2 + +\rho^- c_s^- \rho^+ c_s^+ \|\boldsymbol{n} \times (\boldsymbol{n} \times [\boldsymbol{v}])\|^2\right\} d\boldsymbol{x} + \int_{\mathsf{D}^e,N} \mathfrak{g}^e \cdot \mathfrak{p}^e\, d\boldsymbol{x},\end{aligned}$$

where terms involving k_1 are zero for a face either on or adjacent to the acoustic side. Similarly, for the electromagnetic case

$$\begin{aligned}\sum_e \frac{d}{dt}\mathcal{E}_d^e = &\sum_e \int_{\mathsf{D}^e,N} \mathfrak{g}^e \cdot \mathfrak{p}^e\, d\boldsymbol{x} \\ &- \frac{1}{2}\int_{\partial\mathsf{D}^e,N} \frac{1}{2\,\{\{Z\}\}} \|\boldsymbol{n} \times \boldsymbol{n} \times [\boldsymbol{E}]\|^2 + \frac{1}{2\,\{\{Y\}\}} \|\boldsymbol{n} \times \boldsymbol{n} \times [\boldsymbol{H}]\|^2\, d\boldsymbol{x},\end{aligned}$$

where terms involving $\boldsymbol{E}$ and $\boldsymbol{H}$ vanish for PMC and PEC boundaries, respectively, and both vanish for dielectric boundaries.

Now, for $\mathfrak{g} = 0$ the overall energy is non-increasing, i.e.,

$$\frac{d}{dt}\mathcal{E}_d \le 0.$$

For $\mathfrak{g} \neq 0$, we obtain the following estimate, by Cauchy-Schwarz and Young inequalities,

$$\frac{d}{dt}\mathcal{E}_d \le \int_{\mathcal{D}^{N_{\text{el}}}} \mathfrak{g} \cdot \mathfrak{p} \le \frac{1}{2}\left(\mathcal{E}_d + \|\mathcal{I}_N\boldsymbol{g}\|^2_{\mathcal{D}^{N_{\text{el}}},d}\right).$$

□

5. Mortar-based non-conforming approximations.

In this section, we employ the mortar-based approximation idea proposed by Kopriva *et al.* [14, 18]. However, we propose to use a discretized mortar-based approximation to show stability in addition to the outflow condition and global conservation as required by the original mortar method [14, 18]. As will be shown, our discrete version requires a special quadrature rule in order to simultaneously satisfy all the requirements. We provide a setting that allows unified proofs that are valid for both functional (due to order refinement) and geometric (due to local subdivision) non-conforming approximations.

The following conventions are adopted. We use bold face type to denote vectors of nodal values of the corresponding quantities under consideration. For example, $\mathbf{q}$ is the vector of nodal values of $\mathfrak{q}$. In addition, we use upper case script type to denote matrices, e.g. $\mathscr{P}$.

We consider non-conforming approximations due to domain subdivision in which elements may be subdivided locally while their neighbors may not. For simplicity of exposition, we further restrict ourselves to the case where a subdomain interface between two adjacent elements (two elements are said to be *adjacent* to each other if their boundary intersection has non-zero two-dimensional Lebesgue measure) must be an entire face of either of them. Nevertheless, adjacent elements are allowed to have different solution orders, and hence order refinement (i.e., p-refinement) in addition to domain subdivision (i.e., h-refinement) is permissible. From here on, by "non-conforming interface" we mean that an entire face of one element is also a union of faces of other adjacent elements (h-non-conforming), or, the solution orders of two elements sharing a face are different (p-non-conforming). A non-conforming interface with one element on one side and seven elements on the other side is shown in Figure 5.1.

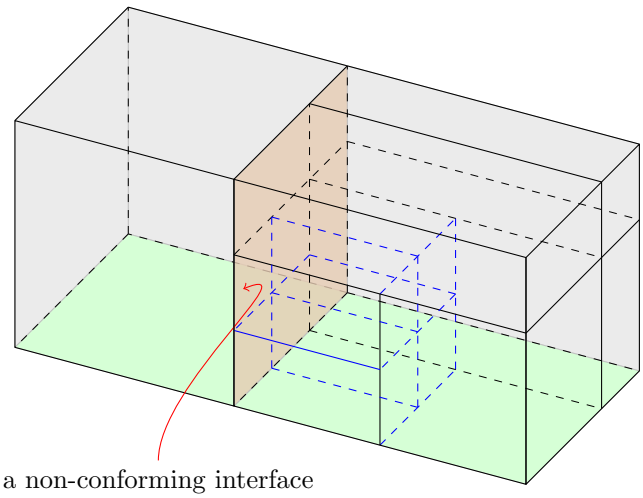

FIG. 5.1. *A non-conforming interface with one hexahedron on one side and seven hexahedra on the other side.*

Consider a non-conforming interface where on the "−" side is face f_{e_0} of element e_0 and on the "+" side are faces f_{e_i} of elements $e_i, i = 1, \ldots, N_a$. Clearly, this setting includes both kinds of non-conforming interfaces. We create N_a mortars $\mathcal{M}_i, i = 1, \ldots, N_a$ whose "−" sides are seen by element e_0 and "+" sides by elements

e_i, respectively. As in [18], the geometric order on the mortars must be the lowest geometric order of the contributing elements, and the polynomial should be defined along face f_{e_0}. This will ensure that the mortars match sub-interfaces between elements exactly, and hence the metrics $J^{e_i}\boldsymbol{a}^{e_i}$ on a mortar and the corresponding contributing element faces are represented by identical polynomials. The solution orders of the mortars are chosen as $N_{m_i} \geq \max\{N_{e_0}, N_{e_i}\}$ which is sufficient to satisfy the outflow condition, as we shall show. An example with seven mortars corresponding to the non-conforming interface in Figure 5.1 is shown in Figure 5.2.

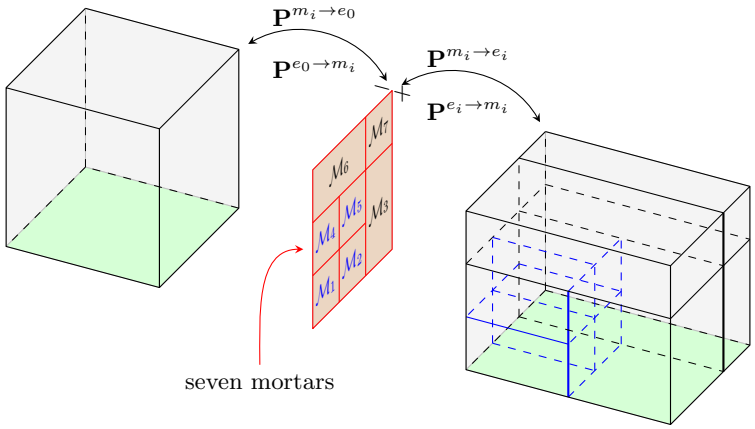

FIG. 5.2. *Seven mortars corresponding to the non-conforming interface in Figure 5.1.*

The goal of the mortar approximation is to compute the contravariant fluxes on faces $f_{e_i}, i = 0, \ldots, N_a$. This is a three-step process. First, the states on e_0 and e_i are projected on the mortars through L^2 projectors $\mathscr{P}^{e_0\to m_i}$ and $\mathscr{P}^{e_i\to m_i}$, $i = 1, \ldots, N_a$. The projected states are then used to compute the mortar contravariant fluxes as if each mortar is a conforming face. The final step is to project the contravariant fluxes back on the element faces using projectors $\mathscr{P}^{m_i\to e_0}$ and $\mathscr{P}^{m_i\to e_i}$. The illustration of steps 1 and 3 can be seen in Figure 5.2. The components of each step are now detailed.

State $\mathfrak{q}^{m_i^-}$ on the "$-$" side of mortar $\mathcal{M}_i$ is the least squares projection of state $\mathfrak{q}^{e_0}$ from element e_0 onto space $\mathcal{P}_{N_{m_i}}$, i.e.,

$$\int_{\mathcal{M}_i} \mathfrak{q}^{m_i^-}(\boldsymbol{r})\,\boldsymbol{\ell}_k^{m_i}(\boldsymbol{r})\,d\boldsymbol{r} = \int_{\mathcal{M}_i} \mathfrak{q}^{e_0}\left((\boldsymbol{X}^{e_0})^{-1}\circ\boldsymbol{X}^{e_i}(\boldsymbol{r})\right)\boldsymbol{\ell}_k^{m_i}(\boldsymbol{r})\,d\boldsymbol{r}, \quad \forall \boldsymbol{\ell}_k^{m_i}(\boldsymbol{r}) \in \mathcal{P}_{N_{m_i}}. \tag{5.1}$$

Since our main goal is to prove semi-stability, least squares projection of the type (5.1) is approximated using quadratures. Nevertheless, we do not wish to violate the outflow condition and global conservation. In fact, the outflow condition is necessary to ensure stability, as shown in §6. In this paper, the following quadrature rule is used. For any surface integral in the least squares projection of the type (5.1), the quadrature rule is chosen to correspond to the integrand with the highest order. For example, the N_{m_i}th-order quadrature rule is used for both integrals in (5.1). Explicitly, we

approximate (5.1) as

$$\int_{\mathcal{M}_i,N_{m_i}} \mathfrak{q}^{m_i^-}(\boldsymbol{r})\,\boldsymbol{\ell}_k^{m_i}(\boldsymbol{r})\,d\boldsymbol{r} = \int_{\mathcal{M}_i,N_{m_i}} \mathfrak{q}^{e_0}\left((\boldsymbol{X}^{e_0})^{-1}\circ\boldsymbol{X}^{e_i}(\boldsymbol{r})\right)\boldsymbol{\ell}_k^{m_i}(\boldsymbol{r})\,d\boldsymbol{r},\quad \forall\boldsymbol{\ell}_k^{m_i}(\boldsymbol{r})\in\mathcal{P}_{N_{m_i}}, \tag{5.2}$$

which yields

$$\mathbf{q}^{m_i^-} = \underbrace{(\mathscr{M}^{m_i})^{-1}\mathscr{R}^{e_0\to m_i}}_{\mathscr{P}^{e_0\to m_i}}\mathbf{q}^{e_0}$$

where the matrices $\mathscr{M}^{m_i}$ and $\mathscr{R}^{e_0\to m_i}$ are defined as

$$\mathscr{M}^{m_i}_{k_1,k_2} = \int_{\mathcal{M}_i,N_{m_i}} \boldsymbol{\ell}_{k_1}^{m_i}(\boldsymbol{r})\,\boldsymbol{\ell}_{k_2}^{m_i}(\boldsymbol{r})\,d\boldsymbol{r},$$
$$\mathscr{R}^{e_0\to m_i}_{k,j} = \int_{\mathcal{M}_i,N_{m_i}} \boldsymbol{\ell}_k^{m_i}(\boldsymbol{r})\,\boldsymbol{\ell}_j^{e_0}\left((\boldsymbol{X}^{e_0})^{-1}\circ\boldsymbol{X}^{e_i}(\boldsymbol{r})\right)d\boldsymbol{r},\quad \forall\boldsymbol{\ell}_j^{e_0}\in\mathcal{P}_{N_{e_0}}.$$

Similarly, the least squares projection of state $\mathfrak{q}^{e_i}$ from element e_i onto $\mathcal{P}_{N_{m_i}}$ is state $\mathfrak{q}^{m_i^+}$ on the "+" side of mortar $\mathcal{M}_i$. Using the above quadrature rule we have

$$\int_{\mathcal{M}_i,N_{m_i}} \mathfrak{q}^{m_i^+}(\boldsymbol{r})\,\boldsymbol{\ell}_k^{m_i}(\boldsymbol{r})\,d\boldsymbol{r} = \int_{\mathcal{M}_i,N_{m_i}} \mathfrak{q}^{e_i}(\boldsymbol{r})\,\boldsymbol{\ell}_k^{m_i}(\boldsymbol{r})\,d\boldsymbol{r},\quad \forall\boldsymbol{\ell}_k^{m_i}(\boldsymbol{r})\in\mathcal{P}_{N_{m_i}}, \tag{5.3}$$

or, equivalently,

$$\mathbf{q}^{m_i^+} = \underbrace{(\mathscr{M}^{m_i})^{-1}\mathscr{R}^{e_i\to m_i}}_{\mathscr{P}^{e_i\to m_i}}\mathbf{q}^{e_i} \tag{5.4}$$

with $\mathscr{R}^{e_i\to m_i}$ defined as

$$\mathscr{R}^{e_i\to m_i}_{k,j} = \int_{\mathcal{M}_i,N_{m_i}} \boldsymbol{\ell}_k^{m_i}(\boldsymbol{r})\,\boldsymbol{\ell}_j^{e_i}(\boldsymbol{r})\,d\boldsymbol{r},\quad \forall\boldsymbol{\ell}_j^{e_i}\in\mathcal{P}_{N_{e_i}}.$$

Since the fluxes depend on λ,μ,ε, and μ, we perform the above least squares projection procedure on them as well. Based on the projected states $\mathfrak{q}^{m_i^-}$, $\mathfrak{q}^{m_i^+}$, and projected coefficients, we compute the contravariant Riemann fluxes $\tilde{\mathfrak{F}}^*_{m_i} = \left(\tilde{\boldsymbol{n}}\cdot\tilde{\mathfrak{F}}\left(\mathfrak{q}^{m_i}\right)\right)^*$ on the mortars as if the mortars are conforming faces. This is done using a simple relation between the contravariant and covariant Riemann fluxes as in [16]. The projected states are also used to compute the contravariant fluxes $\tilde{\mathfrak{F}}^-_{m_i} = \tilde{\boldsymbol{n}}\cdot\tilde{\mathfrak{F}}\left(\mathfrak{q}^{m_i^-}\right)$, and $\tilde{\mathfrak{F}}^+_{m_i} = \tilde{\boldsymbol{n}}\cdot\tilde{\mathfrak{F}}\left(\mathfrak{q}^{m_i^+}\right)$. The final step is to project the mortar contravariant fluxes $\tilde{\mathfrak{F}}^*_{m_i}, \tilde{\mathfrak{F}}^-_{m_i}$ and $\tilde{\mathfrak{F}}^+_{m_i}$ onto $\mathcal{P}_{N_{e_i}}, i=0,\ldots,N_a$. Since the procedure is the same for $\tilde{\mathfrak{F}}^*_{m_i}, \tilde{\mathfrak{F}}^-_{m_i}$ and $\tilde{\mathfrak{F}}^+_{m_i}$, we describe only the process of projecting $\tilde{\mathfrak{F}}^*_{m_i}$ to obtain the contravariant fluxes $\tilde{\mathfrak{F}}^*_{e_i}$ on faces f_{e_i} of the contributing elements. The discretized least squares projection using the quadrature rule discussed above for face f_{e_0} is as follows:

$$\int_{f_{e_0},N_{e_0}} \tilde{\mathfrak{F}}^*_{e_0}(\boldsymbol{r})\,\boldsymbol{\ell}_j^{e_0}(\boldsymbol{r})\,d\boldsymbol{r} = \sum_{i=1}^{N_a}\int_{\mathcal{M}_i,N_{m_i}} \tilde{\mathfrak{F}}^*_{m_i}(\boldsymbol{r})\,\boldsymbol{\ell}_j^{e_0}\left((\boldsymbol{X}^{e_0})^{-1}\circ\boldsymbol{X}^{e_i}(\boldsymbol{r})\right)d\boldsymbol{r},\quad \forall\boldsymbol{\ell}_j^{e_0}\in\mathcal{P}_{N_{e_0}}, \tag{5.5}$$

for which, in matrix notation, the vector of nodal values of $\tilde{\mathfrak{F}}^*_{e_0}$, $\tilde{\mathbf{F}}^*_{e_0}$, is computed as

$$\mathscr{M}^{e_0}\tilde{\mathbf{F}}^*_{e_0} = \sum_{i=1}^{N_a} \mathscr{R}^{m_i\to e_0}\tilde{\mathbf{F}}^*_{m_i},$$

or in terms of projection matrices,

$$\tilde{\mathbf{F}}^*_{e_0} = \sum_{i=1}^{N_a} \underbrace{\left(\mathscr{M}^{e_0}\right)^{-1}\mathscr{R}^{m_i\to e_0}}_{\mathscr{P}^{m_i\to e_0}}\tilde{\mathbf{F}}^*_{m_i}, \tag{5.6}$$

where

$$\mathscr{M}^{e_0}_{k,j} = \int_{\mathcal{M}_i,N_{e_0}} \boldsymbol{\ell}^{e_0}_k(\boldsymbol{r})\,\boldsymbol{\ell}^{e_0}_j(\boldsymbol{r})\,d\boldsymbol{r}, \quad \mathscr{R}^{m_i\to e_0} = \left(\mathscr{R}^{e_0\to m_i}\right)^T. \tag{5.7}$$

Similarly, the vector of nodal values of $\tilde{\mathfrak{F}}^-_{e_0}$, $\tilde{\mathbf{F}}^-_{e_0}$ is given by

$$\tilde{\mathbf{F}}^-_{e_0} = \sum_{i=1}^{N_a} \mathscr{P}^{m_i\to e_0}\tilde{\mathbf{F}}^-_{m_i}. \tag{5.8}$$

The projection to compute contravariant fluxes $\tilde{\mathfrak{F}}^*_{e_i}$ on surface f_{e_i} $i = 1,\ldots,N_a$ of other contributing elements is simpler,

$$\int_{\mathcal{M}_i,N_{e_i}} \tilde{\mathfrak{F}}^*_{e_i}(\boldsymbol{r})\,\boldsymbol{\ell}^{e_i}_j(\boldsymbol{r})\,d\boldsymbol{r} = \int_{\mathcal{M}_i,N_{m_i}} \tilde{\mathfrak{F}}^*_{m_i}(\boldsymbol{r})\,\boldsymbol{\ell}^{e_i}_j(\boldsymbol{r})\,d\boldsymbol{r} = 0, \quad \forall \boldsymbol{\ell}^{e_i}_j(\boldsymbol{r}) \in \mathcal{P}_{N_{e_i}}, \tag{5.9}$$

which yields

$$\tilde{\mathbf{F}}^*_{e_i} = \underbrace{\left(\mathscr{M}^{e_i}\right)^{-1}\mathscr{R}^{m_i\to e_i}}_{\mathscr{P}^{m_i\to e_i}}\tilde{\mathbf{F}}^*_{m_i}, \tag{5.10}$$

where

$$\mathscr{M}^{e_i}_{k,j} = \int_{\mathcal{M}_i,N_{e_i}} \boldsymbol{\ell}^{e_i}_k(\boldsymbol{r})\,\boldsymbol{\ell}^{e_i}_j(\boldsymbol{r})\,d\boldsymbol{r}, \quad \mathscr{R}^{m_i\to e_i} = \left(\mathscr{R}^{e_i\to m_i}\right)^T. \tag{5.11}$$

Similarly,

$$\tilde{\mathbf{F}}^+_{e_i} = \mathscr{P}^{m_i\to e_i}\tilde{\mathbf{F}}^+_{m_i}. \tag{5.12}$$

Recall that the outflow condition means the invariance of a polynomial function when projected to the mortars and back to the face [14, 18]. We are now in a position to discuss the outflow condition for the above discrete mortar-based approximation.

PROPOSITION 1 (Outflow condition). *Assume* $N_{m_i} \geq \max\{N_{e_0}, N_{e_i}\}$, $i = 1,\ldots,N_a$. *Then the discrete mortar-based approximation with LG quadrature satisfies the strong outflow conditions, namely,*

$$\mathscr{P}^{m_i\to e_i}\mathscr{P}^{e_i\to m_i} = \boldsymbol{I}, \quad i = 1,\ldots,N_a, \tag{5.13}$$

$$\sum_{i=1}^{N_a} \mathscr{P}^{m_i\to e_0}\mathscr{P}^{e_0\to m_i} = \boldsymbol{I}, \tag{5.14}$$

where $\boldsymbol{I}$ *is the identity matrix of appropriate size. On the other hand, discretizations using LGL quadrature satisfy the outflow condition in the following weak sense,*

$$\int_{\mathcal{M}_i,N_{m_i}} \mathfrak{q}^{e_i}(\boldsymbol{r})\,\hat{\boldsymbol{\ell}}\,d\boldsymbol{r} = \int_{\mathcal{M}_i,N_{e_i}} \hat{\mathfrak{q}}^{e_i}(\boldsymbol{r})\,\hat{\boldsymbol{\ell}}\,d\boldsymbol{r}, \quad \forall \hat{\boldsymbol{\ell}} \in \mathcal{P}_{N_{e_i}}, \tag{5.15}$$

and

$$\sum_{i=1}^{N_a} \int_{\mathcal{M}_i,N_{m_i}} \mathfrak{q}^{e_0}\left((\boldsymbol{X}^{e_0})^{-1}\circ\boldsymbol{X}^{e_i}(\boldsymbol{r})\right)\hat{\boldsymbol{\ell}}\left((\boldsymbol{X}^{e_0})^{-1}\circ\boldsymbol{X}^{e_i}(\boldsymbol{r})\right)\,d\boldsymbol{r} = \int_{f_{e_0},N_{e_0}} \hat{\mathfrak{q}}^{e_0}(\boldsymbol{r})\,\hat{\boldsymbol{\ell}}(\boldsymbol{r})\,d\boldsymbol{r}, \quad \forall \hat{\boldsymbol{\ell}} \in \mathcal{P}_{N_{e_0}}, \tag{5.16}$$

where $\hat{\mathfrak{q}}^{e_i}$ *is the result from the projection of* $\mathfrak{q}^{e_i}$ *to* $\mathcal{M}_i$ *and back on* f_{e_i}*, and* $\hat{\mathfrak{q}}^{e_0}$ *the result from the projection of* $\mathfrak{q}^{e_0}$ *to* $\mathcal{M}_i$ *and back on* f_{e_0}*.*

Proof. We first show (5.13). Denote $\mathbf{q}^{m_i^+}$ as the projection of $\mathbf{q}^{e_i}$ on mortar $\mathcal{M}_i$, using (5.3) and (5.9), we have

$$\begin{aligned}
&\int_{\mathcal{M}_i,N_{m_i}} \mathfrak{q}^{m_i^+}(\boldsymbol{r})\,\boldsymbol{\ell}(\boldsymbol{r})\,d\boldsymbol{r} = \int_{\mathcal{M}_i,N_{m_i}} \mathfrak{q}^{e_i}(\boldsymbol{r})\,\boldsymbol{\ell}(\boldsymbol{r})\,d\boldsymbol{r}, \quad \forall \boldsymbol{\ell} \in \mathcal{P}_{N_{m_i}},\\
&\int_{\mathcal{M}_i,N_{m_i}} \mathfrak{q}^{m_i^+}(\boldsymbol{r})\,\hat{\boldsymbol{\ell}}(\boldsymbol{r})\,d\boldsymbol{r} = \int_{\mathcal{M}_i,N_{e_i}} \hat{\mathfrak{q}}^{e_i}(\boldsymbol{r})\,\hat{\boldsymbol{\ell}}(\boldsymbol{r})\,d\boldsymbol{r}, \quad \forall \hat{\boldsymbol{\ell}} \in \mathcal{P}_{N_{e_i}} \subset \mathcal{P}_{N_{m_i}},
\end{aligned}$$

which imply the weak outflow condition (5.15). This weak outflow condition is valid for both LGL and LG quadrature rules. For LG quadrature, however, the weak outflow condition also implies the strong one, namely, $\hat{\mathbf{q}}^{e_i} = \mathbf{q}^{e_i}$, and hence (5.13), since LG quadrature is exact.

For (5.14), denote $\hat{\mathfrak{q}}^{m_i^-}$ as the projection of $\mathfrak{q}^{e_0}$ onto mortars $\mathcal{M}_i$. Equations (5.2) and (5.5) imply, for $i = 1,\ldots,N_a$,

$$\begin{aligned}
&\int_{\mathcal{M}_i,N_{m_i}} \mathfrak{q}^{m_i^-}(\boldsymbol{r})\,\boldsymbol{\ell}(\boldsymbol{r})\,d\boldsymbol{r} =\\
&\int_{\mathcal{M}_i,N_{m_i}} \mathfrak{q}^{e_0}\left((\boldsymbol{X}^{e_0})^{-1}\circ\boldsymbol{X}^{e_i}(\boldsymbol{r})\right)\boldsymbol{\ell}(\boldsymbol{r})\,d\boldsymbol{r}, \quad \forall \boldsymbol{\ell} \in \mathcal{P}_{N_{m_i}}, \qquad (5.17)\\
&\sum_{j=1}^{N_a} \int_{\mathcal{M}_j,N_{m_j}} \mathfrak{q}^{m_j^-}(\boldsymbol{r})\,\hat{\boldsymbol{\ell}}\left((\boldsymbol{X}^{e_0})^{-1}\circ\boldsymbol{X}^{e_j}(\boldsymbol{r})\right)\,d\boldsymbol{r} =\\
&\int_{f_{e_0},N_{e_0}} \hat{\mathfrak{q}}^{e_0}(\boldsymbol{r})\,\hat{\boldsymbol{\ell}}(\boldsymbol{r})\,d\boldsymbol{r}, \quad \forall \hat{\boldsymbol{\ell}} \in \mathcal{P}_{N_{e_0}}. \qquad (5.18)
\end{aligned}$$

Since $N_{m_i} \geq \max\{N_{e_0}, N_{e_i}\}$, and hence $\mathcal{P}_{N_{e_0}} \subset \mathcal{P}_{N_{m_i}}$, $i = 1,\ldots,N_a$, we take $\boldsymbol{\ell}(\boldsymbol{r}) = \hat{\boldsymbol{\ell}}\left((\boldsymbol{X}^{e_0})^{-1}\circ\boldsymbol{X}^{e_i}(\boldsymbol{r})\right)$ in (5.17) and sum over $i = 1,\ldots,N_a$, and finally subtract from (5.18) to obtain the weak outflow condition (5.16). Again, by the exactness of LG quadrature we have $\hat{\mathbf{q}}^{e_0} = \mathbf{q}^{e_0}$, and hence (5.14). ∎

REMARK 1. *It is clear that if* $N_{m_i} = N_{e_0} = N_{e_i}$*, i.e., only h non-conformity is considered, the weak outflow conditions are indeed strong.*

PROPOSITION 2 (Global conservation). *The discrete mortar-based approximation satisfies the following global conservation,*

$$\int_{f_{e_0}} \tilde{\mathfrak{F}}^*_{e_0}\, d\boldsymbol{r} = \sum_{i=1}^{N_a} \int_{f_{e_i}} \tilde{\mathfrak{F}}^*_{e_i}\, d\boldsymbol{r}.$$

Proof. This result is an easy consequence of (5.5) and (5.9). Indeed, taking $\boldsymbol{\ell}^{e_0} \equiv 1$ in (5.5) and $\boldsymbol{\ell}^{e_i}_j \equiv 1$ in (5.9), we have

$$\int_{f_{e_0},N_{e_0}} \tilde{\mathfrak{F}}^*_{e_0}(\boldsymbol{r})\, d\boldsymbol{r} = \sum_{i=1}^{N_a} \int_{\mathcal{M}_i,N_{m_i}} \tilde{\mathfrak{F}}^*_{m_i}(\boldsymbol{r})\, d\boldsymbol{r},$$

and

$$\sum_{i=1}^{N_a} \int_{\mathcal{M}_i,N_{e_i}} \tilde{\mathfrak{F}}^*_{e_i}(\boldsymbol{r})\, d\boldsymbol{r} = \sum_{i=1}^{N_a} \int_{\mathcal{M}_i,N_{m_i}} \tilde{\mathfrak{F}}^*_{m_i}(\boldsymbol{r})\, d\boldsymbol{r}.$$

Observe that $\tilde{\mathfrak{F}}^*_{e_0}(\boldsymbol{r})$ is a polynomial of order at most N_{e_0}, while $\tilde{\mathfrak{F}}^*_{e_i}(\boldsymbol{r})$ is a polynomial of order at most N_{e_i}. The exactness of either LGL or LG quadrature completes the proof. ∎

6. Semi-discrete stability for non-conforming meshes. We start this section with a discussion on why the outflow condition is necessary for the stability proof to hold. The semi-discrete form (3.2) is also applied for non-conforming approximation using the mortar method in §5. However, the contravariant fluxes $\left(\tilde{\mathfrak{F}}\mathfrak{q}^e\right)^*$ and $\tilde{\mathfrak{F}}\mathfrak{q}^e$ on the boundary $\partial\hat{\mathsf{D}}$ are the projected values of the mortar contravariant fluxes instead of the trace of the flux, $\tilde{\mathfrak{F}}\mathfrak{q}^e\Big|_{\partial\hat{\mathsf{D}}}$. Accordingly, using commutativity of quadrature and integration by parts [24, 17], (3.2) becomes

$$\begin{aligned}
&\sum_e \int_{\hat{\mathsf{D}},N_e} J^e \mathcal{Q}^e \frac{\partial \mathfrak{q}^e}{\partial t} \cdot \mathfrak{p}^e\, d\boldsymbol{r} - \int_{\hat{\mathsf{D}},N_e} \mathcal{I}_{N_e}\left(\tilde{\mathfrak{F}}\mathfrak{q}^e\right) \cdot \nabla_{\boldsymbol{r}} \cdot \mathfrak{p}^e\, d\boldsymbol{r} \\
&+ \int_{\partial\hat{\mathsf{D}},N_e} \tilde{\boldsymbol{n}} \cdot \left[\left(\tilde{\mathfrak{F}}\mathfrak{q}^e\right)^* - \tilde{\mathfrak{F}}\mathfrak{q}^e + \tilde{\mathfrak{F}}\mathfrak{q}^e\Big|_{\partial\hat{\mathsf{D}}}\right] \cdot \mathfrak{p}^e\, d\boldsymbol{r} = \sum_e \int_{\hat{\mathsf{D}},N_e} J^e \mathfrak{g}^e \cdot \mathfrak{p}^e\, d\boldsymbol{r}. \qquad (6.1)
\end{aligned}$$

conforming approximation, one has $\tilde{\mathfrak{F}}\mathfrak{q}^e\Big|_{\partial\hat{\mathsf{D}}} - \tilde{\mathfrak{F}}\mathfrak{q}^e = 0, \forall \boldsymbol{r} \in \partial\hat{\mathsf{D}}$, and this is the reason why (4.1) holds. This no longer holds for the non-conforming approximation unless $\tilde{\mathfrak{F}}\mathfrak{q}^e = \tilde{\mathfrak{F}}\mathfrak{q}^e\Big|_{\partial\hat{\mathsf{D}}}, \forall \boldsymbol{r} \in \partial\hat{\mathsf{D}}$, which is true if the outflow condition is satisfied and $\tilde{\mathfrak{F}}\mathfrak{q}^e \in \mathcal{P}_{N^e}$. A sufficient condition for $\tilde{\mathfrak{F}}\mathfrak{q}^e \in \mathcal{P}_{N^e}$ to hold is that the medium properties, i.e., λ, μ, and ε, are element-wise constant.

We introduce the global interpolation operator Π whose restriction on element D^e is

$$\Pi|_{\mathsf{D}^e} = \mathcal{I}_{N_e},$$

which allows us to obtain the following stability proof for our non-conforming approximation.

THEOREM 2 (Stability for non-conforming meshes with LG quadratures). *Assume*

(i) *The discrete mortar approach in §5 is used for non-conforming approximations.*
(ii) *The mesh is affine.*
(iii) *The LG quadrature is used, i.e., the strong outflow condition is satisfied.*
(iv) λ, μ, *and* ε, *are element-wise constant.*

Then the DGSEM discretization is stable in the sense that

$$\frac{d}{dt}\mathcal{E}_d \leq \frac{1}{2}\left(\mathcal{E}_d + \|\Pi \mathfrak{g}\|^2_{\mathcal{D}^{N_{el}},d}\right).$$

Moreover, if $\mathfrak{g} = 0$, *then* $\frac{d}{dt}\mathcal{E}_d \leq 0$.

Proof. As discussed above, assumptions (iii) and (iv) imply the identity $\tilde{\mathfrak{F}}\mathfrak{q}^e\Big|_{\partial\hat{\mathsf{D}}} - \tilde{\mathfrak{F}}\mathfrak{q}^e = 0, \forall \boldsymbol{r} \in \partial\hat{\mathsf{D}}$. Therefore, similar to the proof of Theorem 1, we substitute $\mathfrak{p} := \begin{pmatrix} \boldsymbol{S} \\ \boldsymbol{v} \end{pmatrix} := \begin{pmatrix} \mathsf{C}\boldsymbol{E} \\ \boldsymbol{v} \end{pmatrix}$ for the elastic-acoustic case and $\mathfrak{p} = \mathfrak{q}$ for the electromagnetic case, to obtain

$$\sum_e \frac{d}{dt}\mathcal{E}^e_d = \sum_e -\int_{\partial\hat{\mathsf{D}},N_e} \tilde{\boldsymbol{n}} \cdot \left[\left(\tilde{\mathfrak{F}}\mathfrak{q}^e\right)^* - \frac{1}{2}\left(\tilde{\mathfrak{F}}\mathfrak{q}^e\right)\right] \cdot \mathfrak{p}^e \, d\boldsymbol{r} + \int_{\hat{\mathsf{D}},N_e} J^e \mathfrak{g}^e \cdot \mathfrak{p}^e \, d\boldsymbol{r}. \quad (6.2)$$

We divide the surface integrals into two groups, namely, surface integrals associated with conforming and with non-conforming interfaces. The former group has been shown to be non-positive as in the proof of Theorem 1. We therefore need to consider only the latter group for which we take a typical non-conforming interface and its contributing surface integrals as in §5. We shall show that the non-conforming contribution is also non-positive.

The surface integral contributed from element e_0, with the contravariant fluxes projected from mortars, can be written as

$$\begin{aligned}
&-\textstyle\int_{f_{e_0},N^{e_0}} \left[\tilde{\mathfrak{F}}^*_{e_0} - \frac{1}{2}\tilde{\mathfrak{F}}^-_{e_0}\right] \cdot \mathfrak{p}^{e_0} \, d\boldsymbol{r} \\
&= -\left(\mathbf{p}^{e_0}\right)^T \mathbf{M}^{e_0} \left[\tilde{\mathbf{F}}^*_{e_0} - \tfrac{1}{2}\tilde{\mathbf{F}}^-_{e_0}\right] && \text{using quadrature} \\
&= -\textstyle\sum_{i=1}^{N_a} \left(\mathbf{p}^{e_0}\right)^T \mathscr{R}^{m_i \to e_0} \left[\tilde{\mathbf{F}}^*_{m_i} - \tfrac{1}{2}\tilde{\mathbf{F}}^-_{m_i}\right] && \text{using (5.6) and (5.8)} \\
&= -\textstyle\sum_{i=1}^{N_a} \left(\mathbf{p}^{m_i^-}\right)^T \mathscr{M}^{m_i} \left[\tilde{\mathbf{F}}^*_{m_i} - \tfrac{1}{2}\tilde{\mathbf{F}}^-_{m_i}\right] && \text{using (5.3) and (5.7)} \\
&= -\textstyle\sum_{i=1}^{N_a} \int_{\mathcal{M}_i,N_{m_i}} \left[\tilde{\mathfrak{F}}^*_{m_i} - \frac{1}{2}\tilde{\mathfrak{F}}^-_{m_i}\right] \cdot \mathfrak{p}^{m_i^-} \, d\boldsymbol{r} && \text{using quadrature} \\
&= -\textstyle\sum_{i=1}^{N_a} \int_{\mathcal{M}_i,N_{m_i}} \tilde{\boldsymbol{n}} \cdot \left[\left(\tilde{\mathfrak{F}}\left(\mathfrak{q}^{m_i}\right)\right)^* - \frac{1}{2}\tilde{\mathfrak{F}}\left(\mathfrak{q}^{m_i^-}\right)\right] \cdot \mathfrak{p}^{m_i^-} \, d\boldsymbol{r}. && \text{by definition}
\end{aligned}$$

For each contributing element $e_i, i = 1, \ldots, N_a$, the surface integral on face f_{e_i}, with the contravariant fluxes projected from mortars, is

$$\begin{aligned}
&-\textstyle\int_{f_{e_i},N^{e_i}} \left[\tilde{\mathfrak{F}}^*_{e_i} - \frac{1}{2}\tilde{\mathfrak{F}}^-_{e_i}\right] \cdot \mathfrak{p}^{e_i} \, d\boldsymbol{r} \\
&= -\left(\mathbf{p}^{e_i}\right)^T \mathbf{M}^{e_i} \left[\tilde{\mathbf{F}}^*_{e_i} - \tfrac{1}{2}\tilde{\mathbf{F}}^-_{e_i}\right] && \text{using quadrature} \\
&= -\left(\mathbf{p}^{e_i}\right)^T \mathscr{R}^{m_i \to e_i} \left[\tilde{\mathbf{F}}^*_{m_i} - \tfrac{1}{2}\tilde{\mathbf{F}}^+_{m_i}\right] && \text{using (5.10) and (5.12)} \\
&= -\left(\mathbf{p}^{m_i^+}\right)^T \mathscr{M}^{m_i} \left[\tilde{\mathbf{F}}^*_{m_i} - \tfrac{1}{2}\tilde{\mathbf{F}}^+_{m_i}\right] && \text{using (5.4) and (5.11)} \\
&= -\textstyle\int_{\mathcal{M}_i,N_{m_i}} \left[\tilde{\mathfrak{F}}^*_{m_i} - \frac{1}{2}\tilde{\mathfrak{F}}^+_{m_i}\right] \cdot \mathfrak{p}^{m_i^+} \, d\boldsymbol{r} && \text{using quadrature} \\
&= -\textstyle\int_{\mathcal{M}_i,N_{m_i}} \tilde{\boldsymbol{n}} \cdot \left[\left(\tilde{\mathfrak{F}}\left(\mathfrak{q}^{m_i}\right)\right)^* - \frac{1}{2}\tilde{\mathfrak{F}}\left(\mathfrak{q}^{m_i^+}\right)\right] \cdot \mathfrak{p}^{m_i^+} \, d\boldsymbol{r}. && \text{by definition}
\end{aligned}$$

Therefore, we have shown that each non-conforming interface consisting of faces f_{e_i} of contributing elements e_i, $i = 0, \ldots, N_a$, is equivalent to $2N_a$ conforming faces associated with N_a mortars $\mathcal{M}_j$, $j = 1, \ldots, N_a$. That is, the surface integrals in (6.2) in fact consist of conforming interfaces—either the original conforming interfaces or equivalent conforming mortars. The stability proof of Theorem 1 for conforming faces can now be applied to complete the proof. □

When the strong outflow condition is not satisfied, i.e., when LGL quadrature is used as in Proposition 1. We have the following stability.

THEOREM 3 (Stability for non-conforming meshes with LGL quadratures). *Suppose all assumptions in Theorem 2 hold except that the LGL quadrature is employed. Then the DGSEM discretization is stable in the sense that*

$$\frac{d}{dt}\mathcal{E}_d \leq \frac{1}{2}\left((1+2c)\,\mathcal{E}_d + \|\Pi \mathfrak{g}\|^2_{\mathcal{D}^{N_{el}},d}\right),$$

where the small constant c converges to zero if the exact solution $\mathfrak{q}$ is sufficiently smooth.

Proof. When the numerical integration is not exact, we have the following extra term

$$\sum_e \int_{\partial \hat{\mathsf{D}},N_e} \tilde{\boldsymbol{n}} \cdot \left[\tilde{\mathfrak{F}}\mathfrak{q}^e\Big|_{\partial\hat{\mathsf{D}}} - \tilde{\mathfrak{F}}\mathfrak{q}^e\right] \cdot \mathfrak{p}^e \, d\boldsymbol{r}, \tag{6.3}$$

which can be shown to be small as

$$\sum_e \int_{\partial \hat{\mathsf{D}},N_e} \tilde{\boldsymbol{n}} \cdot \left[\tilde{\mathfrak{F}}\mathfrak{q}^e\Big|_{\partial\hat{\mathsf{D}}} - \tilde{\mathfrak{F}}\mathfrak{q}^e\right] \cdot \mathfrak{p}^e \, d\boldsymbol{r} \leq c\mathcal{E}_d. \tag{6.4}$$

We now provide an explicit estimate for the constant c to show that c is indeed negligible. It is sufficient to estimate the error for contributing element e_i whose face f_{e_i} is on the "+" side of a mortar. From the weak outflow identity (5.15) and the triangle inequality, we have

$$\begin{aligned}
&\left|\int_{e_i,N_{e_i}} \tilde{\boldsymbol{n}} \cdot \left[\tilde{\mathfrak{F}}\mathfrak{q}^{e_i}\Big|_{\partial\hat{\mathsf{D}}} - \tilde{\mathfrak{F}}\mathfrak{q}^{e_i}\right] \cdot \mathfrak{p}^{e_i} \, d\boldsymbol{r}\right| \leq \\
&\left|\int_{\mathcal{M}_i,N_{m_i}} \tilde{\boldsymbol{n}} \cdot \tilde{\mathfrak{F}}\mathfrak{q}^{e_i}\Big|_{\partial\hat{\mathsf{D}}} \cdot \mathfrak{p}^{e_i} \, d\boldsymbol{r} - \int_{\mathcal{M}_i} \tilde{\boldsymbol{n}} \cdot \tilde{\mathfrak{F}}\mathfrak{q}^{e_i}\Big|_{\partial\hat{\mathsf{D}}} \cdot \mathfrak{p}^{e_i} \, d\boldsymbol{r}\right| \\
&+ \left|\int_{\mathcal{M}_i,N_{e_i}} \tilde{\boldsymbol{n}} \cdot \tilde{\mathfrak{F}}\mathfrak{q}^{e_i}\Big|_{\partial\hat{\mathsf{D}}} \cdot \mathfrak{p}^{e_i} \, d\boldsymbol{r} - \int_{\mathcal{M}_i} \tilde{\boldsymbol{n}} \cdot \tilde{\mathfrak{F}}\mathfrak{q}^{e_i}\Big|_{\partial\hat{\mathsf{D}}} \cdot \mathfrak{p}^{e_i} \, d\boldsymbol{r}\right|.
\end{aligned}$$

Note that both terms on the right side of the preceding inequality are of the same type, namely, the error between LGL quadrature integration and exact integration for polynomial of order $2N_{e_i}$. Since $N_{m_i} \geq N_{e_i}$, we need to estimate only the second term. Using an error estimate from [1] together with Stirling's formula we have

$$\begin{aligned}
&\left|\int_{\mathcal{M}_i,N_{e_i}} \tilde{\boldsymbol{n}} \cdot \tilde{\mathfrak{F}}\mathfrak{q}^{e_i}\Big|_{\partial\hat{\mathsf{D}}} \cdot \mathfrak{p}^{e_i} \, d\boldsymbol{r} - \int_{\mathcal{M}_i} \tilde{\boldsymbol{n}} \cdot \tilde{\mathfrak{F}}\mathfrak{q}^{e_i}\Big|_{\partial\hat{\mathsf{D}}} \cdot \mathfrak{p}^{e_i} \, d\boldsymbol{r}\right| \\
&= \mathcal{O}\left(\frac{N_{e_i}+1}{2N_{e_i}+1}\left(\frac{N_{e_i}-1}{N_{e_i}}\right)^{4N_{e_i}-2}\frac{1}{2^{2N_{e_i}}}h_e^{2N_{e_i}}\right),
\end{aligned}$$

which shows that the error introduced by having the weak outflow condition (instead of the strong one for which the additional error (6.3) is zero) is decaying exponentially with respect to the solution order N_{e_i}, and at the rate $2N_{e_i}$, i.e., $h_e^{2N_{e_i}}$, with respect to h_e. Compared to the optimal error rate with respect to h_e and N_{e_i} in (7.1)–(7.2), the error rate resulting from the weak outflow condition is much smaller. □

REMARK 2. *By virtue of both h and p estimates above, we see that even though the inexactness of the LGL quadrature violates the strong outflow condition and hence generates additional boundary terms when integration by parts is performed, these terms are negligible. From now on, if LGL quadrature is used, we implicitly absorb the additional error terms arising from the weak outflow condition into constant in the convergence estimate, as in Theorem 4, or simply ignore them.*

7. Convergence rate analysis. The previous sections show that our discrete approximations, both conforming and non-conforming, are stable. Together with consistency, to be shown below, our approximations are convergent by the Lax-Ritchmyer equivalence theorem. The direct consequence is that the solution can grow at most exponentially in time, which is typically for Lax-Ritchmyer type of convergence. This kind of convergence result is interesting for theoretical analysis, but may not be appropriate for assessing the actual convergence rate of a numerical method. Fortunately, Hesthaven and Warburton [12] show that a direct convergence analysis is possible, allowing a much better upper bound on the error estimate. We adapt this type of direct convergence analysis to derive *a priori* error bounds for our non-conforming approximations.

Recall that interpolation introduces truncation and aliasing errors [7, 16], and hence interpolation is generally different from projection, which has only truncation error. For sufficiently smooth functions, however, the aliasing error either is spectrally small [7, 11, 16] or can be made equal to zero [12]. Following [12], we shall make no distinction between interpolation and projection in what remains.

The following conventions are used in this section. We reserve $\mathfrak{q}$ for the unknown exact solution, $\mathcal{I}_{N_e}\mathfrak{q}$ for the projection of $\mathfrak{q}$ on $\mathcal{P}_{N_e}$, and $\mathfrak{q}_{N_e}$ the solution of the discrete form (3.2) restricted on element e. In addition, C denotes a generic constant that may have different values in different contexts, $\mathfrak{q}_d$ is defined by $\mathfrak{q}_d|_{\mathsf{D}^e} = \mathfrak{q}_{N_e}$, and finally a dummy variable q lives in different spaces for different inequalities. To begin, we recall the following fundamental *hp* approximation error bounds [2, 3, 4],

$$\|q - \mathcal{I}_{N_e} q\|_{H^r(\mathsf{D}^e)} \leq C \frac{h_e^{\sigma_e - r}}{N_e^{s_e - r}} \|q\|_{H^{s_e}(\mathsf{D}^e)}, \quad 0 \leq r \leq s_e \tag{7.1}$$

$$\|q - \mathcal{I}_{N_e} q\|_{\partial\mathsf{D}^e} \leq C \frac{h_e^{\sigma_e - 1/2}}{N_e^{s_e - 1/2}} \|q\|_{H^{s_e}(\mathsf{D}^e)}, \quad s_e > \frac{1}{2} \tag{7.2}$$

with $h_e = diam\,(\mathsf{D}^e)$, $\sigma_e = \min\{N_e + 1, s_e\}$, and $\|\cdot\|_{H^r(\mathsf{D}^e)}$ denoting the usual Sobolev norm.

For approximation using tensor product LGL quadrature, the following equivalence of the discrete and continuous norm, an extension of the one dimensional version in [11], is useful in passing from the discrete norm to the continuous one and vice versa: $\forall q \in \mathcal{P}_N$,

$$\|q\|_{\hat{\mathsf{D}}} \leq \|q\|_{\hat{\mathsf{D}},N} \leq \left(2 + \frac{1}{N}\right)^{3/2} \|q\|_{\hat{\mathsf{D}}}, \text{ and } \|q\|_{\partial\hat{\mathsf{D}}} \leq \|q\|_{\partial\hat{\mathsf{D}},N} \leq \left(2 + \frac{1}{N}\right) \|q\|_{\partial\hat{\mathsf{D}}}.$$

We first derive the convergence rate for conforming meshes. Since the electromagnetic, acoustic, elastic, and coupled acoustic–elastic wave equations are similar, we analyze the electromagnetic case and leave out details of the others. Denote $T^{\mathfrak{q}} = \left[T^{\boldsymbol{E}}, T^{\boldsymbol{H}}\right]^T$ as the the truncation error that results from substituting the exact solution $\mathfrak{q}$ in the discrete equation (3.2). Using the fact that $\mathfrak{q}$ satisfies the Maxwell's equations, we have

$$\begin{aligned}
\left(\boldsymbol{\ell}_k, \mathcal{I}_{N_e} T^{\boldsymbol{E}}\right)_{\mathsf{D}^e,N_e} &= \left(\boldsymbol{\ell}_k, \mathcal{I}_{N_e}\nabla\times(\boldsymbol{H}-\mathcal{I}_{N_e}\boldsymbol{H})\right)_{\mathsf{D}^e,N_e} \\
&\quad + \left(\boldsymbol{\ell}_k, \frac{1}{2\{\{Z\}\}}\boldsymbol{n}\times\left(Z^+\left[\mathcal{I}_{N_e}\boldsymbol{H}\right]-\boldsymbol{n}\times\left[\mathcal{I}_{N_e}\boldsymbol{E}\right]\right)\right)_{\partial\mathsf{D}^e,N_e}, \quad \forall \boldsymbol{\ell}_k \in \mathcal{P}_{N_e} \\
\left(\boldsymbol{\ell}_k, \mathcal{I}_{N_e} T^{\boldsymbol{H}}\right)_{\mathsf{D}^e,N_e} &= \left(\boldsymbol{\ell}_k, \mathcal{I}_{N_e}\nabla\times(\boldsymbol{E}-\mathcal{I}_{N_e}\boldsymbol{E})\right)_{\mathsf{D}^e,N_e} \\
&\quad + \left(\boldsymbol{\ell}_k, \frac{1}{2\{\{Y\}\}}\boldsymbol{n}\times\left(Y^+\left[\mathcal{I}_{N_e}\boldsymbol{E}\right]+\boldsymbol{n}\times\left[\mathcal{I}_{N_e}\boldsymbol{H}\right]\right)\right)_{\partial\mathsf{D}^e,N_e}, \quad \forall \boldsymbol{\ell}_k \in \mathcal{P}_{N_e}
\end{aligned}$$

where, to the end of this section, μ and ε are assumed to be element-wise constant, and the mesh is affine. Note that since the truncation errors for the electric and magnetic equations are similar, we need to estimate only the former and infer the later. Since $\mathcal{I}_{N_e} T^{\boldsymbol{E}} \in \mathcal{P}_{N_e}$, we can take $\boldsymbol{\ell}_k = \mathcal{I}_{N_e} T^{\boldsymbol{E}}$ and use the Cauchy–Schwarz inequality together with the equivalence of discrete and continuous norms to obtain

$$\begin{aligned}
\left\|\mathcal{I}_{N_e} T^{\boldsymbol{E}}\right\|^2_{\mathsf{D}^e,N_e} &\le 27^2 \left\|\mathcal{I}_{N_e}\nabla\times(\boldsymbol{H}-\mathcal{I}_{N_e}\boldsymbol{H})\right\|_{\mathsf{D}^e} \left\|\mathcal{I}_{N_e} T^{\boldsymbol{E}}\right\|_{\mathsf{D}^e} \\
&\quad + 9^2 \left\|\frac{1}{2\{\{Z\}\}}\boldsymbol{n}\times\left(Z^+\left[\mathcal{I}_{N_e}\boldsymbol{H}\right]-\boldsymbol{n}\times\left[\mathcal{I}_{N_e}\boldsymbol{E}\right]\right)\right\|_{\partial\mathsf{D}^e} \left\|\mathcal{I}_{N_e} T^{\boldsymbol{E}}\right\|_{\partial\mathsf{D}^e}.
\end{aligned}$$

Now using the following inverse trace inequality [23], $\forall q \in \mathcal{P}_{N_e}$,

$$\|q\|_{\partial\mathsf{D}^e} \le C\frac{N_e}{h_e^{1/2}}\|q\|_{\mathsf{D}^e} \tag{7.3}$$

yields

$$\begin{aligned}
\left\|\mathcal{I}_{N_e} T^{\boldsymbol{E}}\right\|_{\mathsf{D}^e,N_e} &\le C\left\|\mathcal{I}_{N_e}\nabla\times(\boldsymbol{H}-\mathcal{I}_{N_e}\boldsymbol{H})\right\|_{\mathsf{D}^e} \\
&\quad + C\frac{N_e}{h_e^{1/2}}\left\|\frac{1}{2\{\{Z\}\}}\left(Z^+\left[\mathcal{I}_{N_e}\boldsymbol{H}_\tau\right]-\left[\mathcal{I}_{N_e}\boldsymbol{E}_\tau\right]\right)\right\|_{\partial\mathsf{D}^e},
\end{aligned} \tag{7.4}$$

where we have introduced the tangent components of $\boldsymbol{E}$ and $\boldsymbol{H}$ as

$$\boldsymbol{E}_\tau = \boldsymbol{n}\times(\boldsymbol{n}\times\boldsymbol{E}), \quad \boldsymbol{H}_\tau = \boldsymbol{n}\times\boldsymbol{H}.$$

We now have the following consistency result.

LEMMA 1 (Consistency). *Suppose that each component $\mathfrak{q}_i^e \in H^{s_e}(\mathsf{D}^e), s_e \ge 3/2$, for $i = 1,\dots,d$, with $d = 6$ for electromagnetic case and $d = 12$ for elastic–acoustic case. Furthermore, assume that μ and ε (λ and μ for elastic–acoustic case) are element-wise constant, and the mesh is affine. There exists a constant C dependent on s, angle condition of D^e, and local values of μ and ε (λ and μ for elastic–acoustic case), but independent of $\mathfrak{q}, h_e$, and N_e such that*

$$\left\|\mathcal{I}_{N_e} T^{\mathfrak{q}}\right\|_{\mathcal{D}^{N_{el}},d} \le C\sum_e \frac{h_e^{\sigma_e-1}}{N_e^{s_e-3/2}}\left\|\mathfrak{q}\right\|_{[H^{s_e}(\mathsf{D}^e)]^d}.$$

Proof. Since the proofs for electromagnetic and elastic–acoustic cases are similar, we provide only the proof for the former. We begin by estimating the bound for the first term on the right side of (7.4). Using approximation result (7.1) we have

$$\|\mathcal{I}_{N_e}\nabla\times(\boldsymbol{H}-\mathcal{I}_{N_e}\boldsymbol{H})\|_{\mathsf{D}^e}\leq\|\nabla\times(\boldsymbol{H}-\mathcal{I}_{N_e}\boldsymbol{H})\|_{\mathsf{D}^e}\leq C\frac{h_e^{\sigma_e-1}}{N_e^{s_e-1}}\|\boldsymbol{H}\|_{[H^{s_e}(\mathsf{D}^e)]^3}\,.$$

To estimate the second term we use the regularity of the exact solution, i.e., the tangent component of the field is continuous, and the triangle inequality to bound $\|[\mathcal{I}_{N_e}\boldsymbol{H}_\tau]\|_{\partial\mathsf{D}^e}$, and hence similarly for $\|[\mathcal{I}_{N_e}\boldsymbol{E}_\tau]\|_{\partial\mathsf{D}^e}$, as

$$\|[\mathcal{I}_{N_e}\boldsymbol{H}_\tau]\|_{\partial\mathsf{D}^e}\leq\left\|\boldsymbol{H}_\tau^- - \mathcal{I}_{N_e}\boldsymbol{H}_\tau^-\right\|_{\partial\mathsf{D}^e}+\left\|\boldsymbol{H}_\tau^+ - \mathcal{I}_{N_e}\boldsymbol{H}_\tau^+\right\|_{\partial\mathsf{D}^e}$$

Two terms of the right side of the preceding inequality are of the same type, and therefore we need to estimate only the bound for the first term. But this is straightforward using (7.2), i.e.,

$$\left\|\boldsymbol{H}_\tau^- - \mathcal{I}_{N_e}\boldsymbol{H}_\tau^-\right\|_{\partial\mathsf{D}^e}\leq C\frac{h_e^{\sigma_e-1/2}}{N_e^{s_e-1/2}}\|\boldsymbol{H}_\tau\|_{[H^{s_e}(\mathsf{D}^e)]^3}\leq C\frac{h_e^{\sigma_e-1/2}}{N_e^{s_e-1/2}}\|\boldsymbol{H}\|_{[H^{s_e}(\mathsf{D}^e)]^3}\,.$$

Now combining the above estimates for both terms on the right side of (7.4), summing over all elements, and using the discrete Hölder inequality completes the proof. ∎

REMARK 3. *Note that the proof of Lemma 1 is carried out for conforming meshes. However, by the proof of Theorem 2, the surface integrals in* (6.2) *in fact consist of conforming interfaces—either the original conforming interfaces or equivalent conforming mortars. Hence, the proof for non-conforming meshes is almost identical except for bounding the boundary terms which are now defined on the mortars instead of on the contributing element faces. But the fields on the mortars are the L^2 orthogonal projections of those on the contributing element faces, which implies L^2 norms of fields on mortars to be at most those on contributing element faces. This shows that the proof for conforming meshes is sufficient.*

We now state the first convergence result.

THEOREM 4. *Assume $\mathfrak{q}^e\in[H^{s_e}(\mathsf{D}^e)]^d, s_e\geq 3/2$ with $d=6$ for electromagnetic case and $d=12$ for elastic–acoustic case. In addition, suppose $\mathfrak{q}_d(0)=\Pi\mathfrak{q}(0)$. Furthermore, assume that μ and ε (λ and μ for elastic–acoustic case) are element-wise constant, and the mesh is affine. Then, the solution $\mathfrak{q}_d$ of the discrete form* (3.2) *converges to the exact solution $\mathfrak{q}$, i.e., there exists a constant C that depends only on the angle condition of D^e, s, and the material constants μ and ε (λ and μ for elastic–acoustic case) such that*

$$\|\mathfrak{q}(t)-\mathfrak{q}_d(t)\|_{\mathcal{D}^{N_{el},d}}\leq C\sum_e\left[\frac{h_e^{\sigma_e}}{N_e^{s_e}}\|\mathfrak{q}(t)\|_{[H^{s_e}(\mathsf{D}^e)]^d}+t\frac{h_e^{\sigma_e-1}}{N_e^{s_e-3/2}}\max_{[0,t]}\|\mathfrak{q}(t)\|_{[H^{s_e}(\mathsf{D}^e)]^d}\right]$$

Proof. We begin the proof with the following identities

$$
\begin{aligned}
&\left(\mathcal{I}_{N_e}\boldsymbol{E}-\boldsymbol{E}_{N_e},\mathcal{I}_{N_e}T^{\boldsymbol{E}}\right)_{\mathsf{D}^e,N_e}=\left(\mathcal{I}_{N_e}\boldsymbol{E}-\boldsymbol{E}_{N_e},\varepsilon\frac{\partial\left(\mathcal{I}_{N_e}\boldsymbol{E}-\boldsymbol{E}_{N_e}\right)}{\partial t}\right)_{\mathsf{D}^e,N_e}\\
&-\left(\mathcal{I}_{N_e}\boldsymbol{E}-\boldsymbol{E}_{N_e},\mathcal{I}_{N_e}\nabla\times\left(\mathcal{I}_{N_e}\boldsymbol{H}-\boldsymbol{H}_{N_e}\right)\right)_{\mathsf{D}^e,N_e}\\
&+\left(\mathcal{I}_{N_e}\boldsymbol{E}-\boldsymbol{E}_{N_e},\frac{1}{2\left\{\{Z\}\right\}}\boldsymbol{n}\times\left(Z^{+}\left[\mathcal{I}_{N_e}\boldsymbol{H}-\boldsymbol{H}_{N_e}\right]-\boldsymbol{n}\times\left[\mathcal{I}_{N_e}\boldsymbol{E}-\boldsymbol{E}_{N_e}\right]\right)\right)_{\partial\mathsf{D}^e,N_e},\\
&\left(\mathcal{I}_{N_e}\boldsymbol{H}-\boldsymbol{H}_{N_e},\mathcal{I}_{N_e}T^{\boldsymbol{H}}\right)_{\mathsf{D}^e,N_e}=\left(\mathcal{I}_{N_e}\boldsymbol{H}-\boldsymbol{H}_{N_e},\mu\frac{\partial\left(\mathcal{I}_{N_e}\boldsymbol{H}-\boldsymbol{H}_{N_e}\right)}{\partial t}\right)_{\mathsf{D}^e,N_e}\\
&+\left(\mathcal{I}_{N_e}\boldsymbol{H}-\boldsymbol{H}_{N_e},\mathcal{I}_{N_e}\nabla\times\left(\mathcal{I}_{N_e}\boldsymbol{E}-\boldsymbol{E}_{N_e}\right)\right)_{\mathsf{D}^e,N_e}\\
&-\left(\mathcal{I}_{N_e}\boldsymbol{H}-\boldsymbol{H}_{N_e},\frac{1}{2\left\{\{Y\}\right\}}\boldsymbol{n}\times\left(Y^{+}\left[\mathcal{I}_{N_e}\boldsymbol{E}-\boldsymbol{E}_{N_e}\right]+\boldsymbol{n}\times\left[\mathcal{I}_{N_e}\boldsymbol{H}-\boldsymbol{H}_{N_e}\right]\right)\right)_{\partial\mathsf{D}^e,N_e},
\end{aligned}
$$

where we have substituted the exact solution into the discrete equation (3.2), and used $\mathcal{I}_{N_e}\boldsymbol{E}-\boldsymbol{E}_{N_e}$ and $\mathcal{I}_{N_e}\boldsymbol{H}-\boldsymbol{H}_{N_e}$ as test functions for the electric and magnetic equations, respectively.

Following the proof of Theorem 2, we integrate the preceding equations by parts, sum up the resulting equations, cancel the volume terms involving the fluxes, and use the non-positiveness of the boundary integrals to arrive at

$$
\frac{d}{dt}\left\|\Pi\mathfrak{q}-\mathfrak{q}_d\right\|^2_{\mathcal{D}^{N_{\mathrm{el}},d}}\leq C\sum_e\left(\mathcal{I}_{N_e}\mathfrak{q}-\mathfrak{q}_{Ne},\mathcal{I}_{N_e}T^{\mathfrak{q}}\right)_{\mathsf{D}^e,N_e},
$$

where we have used the fact that the material constants μ and ε are bounded away from zero. Next, we use Cauchy-Schwarz and then the discrete Hölder inequalities, then apply the consistency result of Lemma 1 to obtain

$$
\frac{d}{dt}\left\|\Pi\mathfrak{q}-\mathfrak{q}_d\right\|_{\mathcal{D}^{N_{\mathrm{el}},d}}\leq C\sum_e\frac{h_e^{\sigma_e-1}}{N_e^{s_e-3/2}}\left\|\mathfrak{q}\right\|_{[H^{s_e}(\mathsf{D}^e)]^d}\leq C\sum_e\frac{h_e^{\sigma_e-1}}{N_e^{s_e-3/2}}\max_{[0,t]}\left\|\mathfrak{q}\right\|_{[H^{s_e}(\mathsf{D}^e)]^d},
$$

which, after integrating in time, yields

$$
\left\|\Pi\mathfrak{q}\left(t\right)-\mathfrak{q}_d\left(t\right)\right\|_{\mathcal{D}^{N_{\mathrm{el}},d}}\leq Ct\sum_e\frac{h_e^{\sigma_e-1}}{N_e^{s_e-3/2}}\max_{[0,t]}\left\|\mathfrak{q}\left(t\right)\right\|_{[H^{s_e}(\mathsf{D}^e)]^d},
$$

where we have used $\mathfrak{q}_d(0)=\Pi\mathfrak{q}(0)$. Now, using the triangle inequality we have,

$$
\left\|\mathfrak{q}\left(t\right)-\mathfrak{q}_d\left(t\right)\right\|_{\mathcal{D}^{N_{\mathrm{el}},d}}\leq\left\|\mathfrak{q}\left(t\right)-\Pi\mathfrak{q}\left(t\right)\right\|_{\mathcal{D}^{N_{\mathrm{el}},d}}+\left\|\Pi\mathfrak{q}\left(t\right)-\mathfrak{q}_d\left(t\right)\right\|_{\mathcal{D}^{N_{\mathrm{el}},d}}.
$$

Finally, using the equivalence of the discrete and continuous norms and (7.1) ends the proof. ∎

REMARK 4. *Since all norms are equivalent in finite dimensional spaces, the result of Theorem 4 holds for other norms as well, with possibly different constant C. In particular, we have*

$$
\sum_e\left\|\mathfrak{q}\left(t\right)-\mathfrak{q}_d\left(t\right)\right\|_{\mathsf{D}^e,N_e}\leq C\sum_e\left[\frac{h_e^{\sigma_e}}{N_e^{s_e}}\left\|\mathfrak{q}\left(t\right)\right\|_{[H^{s_e}(\mathsf{D}^e)]^d}+t\frac{h_e^{\sigma_e-1}}{N_e^{s_e-3/2}}\max_{[0,t]}\left\|\mathfrak{q}\left(t\right)\right\|_{[H^{s_e}(\mathsf{D}^e)]^d}\right].
$$

REMARK 5. *We again emphasize that the LGL quadrature introduces additional error terms when the discrete integration by parts is performed. However, they are shown to be negligible in Theorem 3 and Remark 2, so their absence in the proof of Theorem 4 is justified. The proof for the LG quadrature follows exactly the same line and hence is omitted here. The only difference is that all the numerical integrations are exact, and therefore there is no need to invoke the equivalence of discrete and continuous norms.*

The proof of Theorem 4 is simple since it directly uses the consistency and stability results. Nevertheless, the rate is suboptimal in h by a factor of $1/2$ and in N by 1 compared to the DG literature. This loss is incurred when estimating the truncation error and using the inverse trace inequality (7.3). This begs for a more sophisticated proof that does not lead to a deterioration of the optimal convergence rate. Inspired by the work of Warburton [26], we present a proof that improves the convergence rate in h by a factor of $1/2$ and in N by 1. We start by rewriting (3.2), after integrating by parts, for an affine mesh and element-wise constant materials as

$$\begin{aligned}&\sum_e \int_{\mathsf{D}^e} \frac{\partial \mathfrak{q}_{N_e}}{\partial t} \cdot \mathfrak{p}^e \, d\boldsymbol{x} - \int_{\mathsf{D}^e} \mathfrak{F}\mathfrak{q}_{N_e} \cdot (\nabla_{\boldsymbol{x}} \cdot \mathfrak{p}^e) \, d\boldsymbol{x} \\ &+ \int_{\partial \mathsf{D}^e} \tilde{\boldsymbol{n}} \cdot \left[(\mathfrak{F}\mathfrak{q}_{N_e})^* \right] \cdot \mathfrak{p}^e \, d\boldsymbol{x} = \sum_e \int_{\mathsf{D}^e} \mathfrak{g}^e \cdot \mathfrak{p}^e \, d\boldsymbol{x} + \mathcal{R}_e, \quad \forall \mathfrak{p} \in \mathcal{V}_d, \end{aligned} \tag{7.5}$$

where, by the proof of Theorem 3, $\mathcal{R}_e = o\left(\frac{h_e^{\sigma_e}}{N_e^{s_e}}\right)$ and $\mathcal{R}_e = 0$ for LGL and LG quadratures, respectively. Since the exact solution $\mathfrak{q}$ also satisfies (7.5) with $\mathcal{R}_e = 0$, we obtain

$$\begin{aligned}&\sum_e \int_{\mathsf{D}^e} \frac{\partial \left(\mathfrak{q} - \mathfrak{q}_{N_e}\right)}{\partial t} \cdot \mathfrak{p}^e \, d\boldsymbol{x} - \int_{\mathsf{D}^e} \mathfrak{F}\left(\mathfrak{q} - \mathfrak{q}_{N_e}\right) \cdot (\nabla_{\boldsymbol{x}} \cdot \mathfrak{p}^e) \, d\boldsymbol{x} \\ &+ \int_{\partial \mathsf{D}^e} \tilde{\boldsymbol{n}} \cdot \left(\mathfrak{F}\left(\mathfrak{q} - \mathfrak{q}_{N_e}\right)\right)^* \cdot \mathfrak{p}^e \, d\boldsymbol{x} = -\sum_e \mathcal{R}_e, \quad \forall \mathfrak{p} \in \mathcal{V}_d. \end{aligned} \tag{7.6}$$

Next, adding and subtracting the elemental projection of the exact solution, i.e., $\mathcal{I}_{N_e}\mathfrak{q}$, yield,

$$\begin{aligned}&\sum_e \int_{\mathsf{D}^e} \frac{\partial \left(\mathcal{I}_{N_e}\mathfrak{q} - \mathfrak{q}_{N_e}\right)}{\partial t} \cdot \mathfrak{p}^e \, d\boldsymbol{x} - \int_{\mathsf{D}^e} \mathfrak{F}\left(\mathcal{I}_{N_e}\mathfrak{q} - \mathfrak{q}_{N_e}\right) \cdot (\nabla_{\boldsymbol{x}} \cdot \mathfrak{p}^e) \, d\boldsymbol{x} \\ &+ \int_{\partial \mathsf{D}^e} \tilde{\boldsymbol{n}} \cdot \left(\mathfrak{F}\left(\mathcal{I}_{N_e}\mathfrak{q} - \mathfrak{q}_{N_e}\right)\right)^* \cdot \mathfrak{p}^e \, d\boldsymbol{x} \\ &= -\sum_e \int_{\partial \mathsf{D}^e} \tilde{\boldsymbol{n}} \cdot \left(\mathfrak{F}\left(\mathfrak{q} - \mathcal{I}_{N_e}\mathfrak{q}\right)\right)^* \cdot \mathfrak{p}^e \, d\boldsymbol{x} - \mathcal{R}_e, \quad \forall \mathfrak{p} \in \mathcal{V}_d, \end{aligned} \tag{7.7}$$

where we have used the linearity of $\mathfrak{F}$ and the following orthogonal identity,

$$\int_{\mathsf{D}^e} \left(\mathfrak{q} - \mathcal{I}_{N_e}\mathfrak{q}\right) \cdot \mathfrak{p}^e \, d\boldsymbol{x} = 0, \quad \mathfrak{p}^e \in L^2\left(\mathsf{D}^e\right)^d.$$

Now, integrating (7.7) by parts, testing the resulting equation and (7.7) with $\mathfrak{p}^e =$

$\mathcal{I}_{N_e}\mathfrak{q} - \mathfrak{q}_{N_e}$, and then adding them yield,

$$\frac{d}{dt}\left\|\Pi\mathfrak{q} - \mathfrak{q}_d\right\|^2_{\mathcal{D}^{N_{\text{el}}},d} + \sum_e \frac{1}{2}\int_{\partial \mathsf{D}^e} \tilde{\boldsymbol{n}} \cdot \left(\mathfrak{F}\left(\mathfrak{q} - \mathcal{I}_{N_e}\mathfrak{q}\right)\right)^* \cdot \left[\mathcal{I}_{N_e}\mathfrak{q} - \mathfrak{q}_{N_e}\right] d\boldsymbol{x} + \mathcal{R}_e$$
$$= -\sum_e \underbrace{\int_{\partial \mathsf{D}^e} \tilde{\boldsymbol{n}} \cdot \left[\left(\mathfrak{F}\left(\mathcal{I}_{N_e}\mathfrak{q} - \mathfrak{q}_{N_e}\right)\right)^* - \frac{1}{2}\mathfrak{F}\left(\mathcal{I}_{N_e}\mathfrak{q} - \mathfrak{q}_{N_e}\right)\right] \cdot \left(\mathcal{I}_{N_e}\mathfrak{q} - \mathfrak{q}_{N_e}\right) d\boldsymbol{x}}_{K^e}. \quad (7.8)$$

On the other hand, if ρ, λ, μ and ε are bounded, the proof of Theorems 1 and 2 implies

$$K^e \geq \alpha^e \left\|\left[\mathcal{I}_{N_e}\mathfrak{q} - \mathfrak{q}_{N_e}\right]\right\|^2_{\left[L^2(\partial \mathsf{D}^e)\right]^d}, \quad (7.9)$$

for some $\alpha^e > 0$.

We are now in the position to prove the following convergence result.

THEOREM 5. *Assume $\mathfrak{q}^e \in \left[H^{s_e}\left(\mathsf{D}^e\right)\right]^d, s_e \geq 3/2$ with $d = 6$ for electromagnetic case and $d = 12$ for elastic–acoustic case. In addition, suppose $\mathfrak{q}_d(0) = \Pi\mathfrak{q}(0)$. Furthermore, assume that μ and ε (λ and μ for elastic–acoustic case) are element-wise constant, and the mesh is affine. Then, the solution $\mathfrak{q}_d$ of the discrete form (3.2) converges to the exact solution $\mathfrak{q}$, i.e., there exists a constant C that depends only on the angle condition of D^e, s, and the material constants μ and ε (λ and μ for elastic–acoustic case) such that*

$$\left\|\mathfrak{q}\left(t\right) - \mathfrak{q}_d\left(t\right)\right\|_{\mathcal{D}^{N_{el}},d} \leq C\sum_e \left[\frac{h_e^{\sigma_e}}{N_e^{s_e}}\left\|\mathfrak{q}\left(t\right)\right\|_{\left[H^{s_e}\left(\mathsf{D}^e\right)\right]^d} + t\frac{h_e^{\sigma_e - 1/2}}{N_e^{s_e - 1/2}}\max_{[0,t]}\left\|\mathfrak{q}\left(t\right)\right\|_{\left[H^{s_e}\left(\mathsf{D}^e\right)\right]^d}\right]$$

Proof. Using the Young inequality for some $\beta^e > 0$ we have,

$$\sum_e \int_{\partial \mathsf{D}^e} \left|\tilde{\boldsymbol{n}} \cdot \left(\mathfrak{F}\left(\mathfrak{q} - \mathcal{I}_{N_e}\mathfrak{q}\right)\right)^* \cdot \left[\mathcal{I}_{N_e}\mathfrak{q} - \mathfrak{q}_{N_e}\right]\right| d\boldsymbol{x} \leq \sum_e \beta^e \left\|\mathfrak{q} - \mathcal{I}_{N_e}\mathfrak{q}\right\|^2_{\left[L^2(\partial \mathsf{D}^e)\right]^d}$$
$$+ \sum_e \frac{1}{\beta^e}\left\|\left[\mathcal{I}_{N_e}\mathfrak{q} - \mathfrak{q}_{N_e}\right]\right\|^2_{\left[L^2(\partial \mathsf{D}^e)\right]^d}, \quad (7.10)$$

where we have used the linearity of $\mathfrak{F}^*$. Combining (7.8), (7.9), and (7.10) yields

$$\frac{d}{dt}\left\|\Pi\mathfrak{q} - \mathfrak{q}_d\right\|^2_{\mathcal{D}^{N_{\text{el}}},d} + \sum_e \left(\alpha - \frac{1}{\beta^e}\right)\left\|\left[\mathcal{I}_{N_e}\mathfrak{q} - \mathfrak{q}_{N_e}\right]\right\|^2_{\left[L^2(\partial \mathsf{D}^e)\right]^d}$$
$$\leq \sum_e \beta^e \left\|\mathfrak{q} - \mathcal{I}_{N_e}\mathfrak{q}\right\|^2_{\left[L^2(\partial \mathsf{D}^e)\right]^d} + \left|\mathcal{R}_e\right|. \quad (7.11)$$

Next, taking $\beta^e \geq \frac{1}{\alpha^e}$ and using (7.2) give

$$\frac{d}{dt}\left\|\Pi\mathfrak{q} - \mathfrak{q}_d\right\|^2_{\mathcal{D}^{N_{\text{el}}},d} \leq C\sum_e \frac{h_e^{2\sigma_e - 1}}{N_e^{2s_e - 1}}\max_{[0,t]}\left\|\mathfrak{q}\right\|^2_{\left[H^{s_e}\left(\mathsf{D}^e\right)\right]^d}.$$

The rest of the proof follows similarly to that of Theorem 4. ∎

We have restricted ourselves to the case of affine hexahedral meshes and element-wise constant medium properties. This allows us to eliminate the volume integrals of fluxes on the right side of equation (4.1) since differentiation and interpolation commute. The discrete stability is then apparent due to the non-positiveness of the

surface integrals of fluxes. Most of the results still hold for meshes with $J\boldsymbol{a}^i =$ constant, for $i = 1, 2, 3$. In addition, it is not difficult to see that the stability, and hence convergence, results for both conforming and non-conforming approximations are still valid for meshes with curved elements, provided that the contravariant fluxes are polynomials with order at most N^e, i.e.,

$$\tilde{\mathfrak{F}}^i = J^e \boldsymbol{a}^i \cdot \mathfrak{F} \in \mathcal{P}_{N^e}, \quad i = 1, 2, 3, \tag{7.12}$$

for which we again have the commutativity of differentiation and interpolation. Together with the metric identities in [15], we again can eliminate the volume integrals after integrating by parts. Moreover, it is clear that our results remain true for other types of meshes, e.g., affine tetrahedral meshes as well, as long as the discrete integration by parts is possible and the commutativity of differentiation and interpolation is valid. For general curvilinear hexahedral meshes, it is not clear whether the volume integrals vanish (or become negative) or not since differentiation and interpolation generally do not commute (even over-integration is not helpful in this case).

8. Conclusions. We have presented an analysis of a non-conforming *hp* discontinuous Galerkin spectral element method for time domain solution of wave propagation problems in acoustic, elastic, coupled elastic–acoustic, and electromagnetic media. We have proven consistency, stability, and convergence under the usual assumptions, i.e., affine meshes and element-wise constant medium properties. Our analytical results hold for both exact numerical integration using tensor product Legendre-Gauss quadrature and inexact numerical integration using tensor product Legendre-Gauss-Lobatto quadrature. The key ingredient of our proposed approach is the development of a discrete mortar-based approach for non-conforming approximations. With this mortar construction, we have shown that the proofs for non-conforming cases closely follow those for conforming ones, and the resulting convergence retains the same optimal rate as for standard DG methods. Numerical experiments in [27] for acoustic, elastic, and coupled acoustic-elastic wave propagation on *h*-non-conforming meshes confirm the theoretical rates presented here, and a further companion paper numerically demonstrates optimal convergence for electromagnetic wave propagation [6].

Acknowledgements. We thank Drs. Carsten Burstedde, Georg Stadler, and Lucas Wilcox for many fruitful discussions on their article [27], which stimulated the work presented here. We thank Prof. David Kopriva of Florida State University for his encouragement, without which this article would not have been possible. We also thank Prof. Ivo Babuška for helpful discussions of his approximation results (7.1)–(7.2). Finally, we thank Prof. Tim Warburton for pointing out material in Ref. [26] that inspired us to improve the convergence rate in our proof.

REFERENCES

[1] Milton Abramowitz and Irene A. Stegun, eds., *Handbook of Mathematical Functions with Formulas, Graphs and Mathematical Tables*, Dover, New York, 1965.

[2] Ivo Babuška and Manil Suri, *The hp-version of the finite element method with quasiuniform meshes*, Mathematical Modeling and Numerical Analysis, 21 (1987), pp. 199–238.

[3] ———, *The optimal convergence rate of the p-version of the finite element method*, Siam J. Numer. Anal., 24 (1987), pp. 750–776.

[4] ———, *The p and h − p version of the finite element method, basic principles and properties*, SIAM Review, 36 (1994), pp. 578–632.

[5] Carlos Erik Baumann and John Tinsley Oden, *A discontinuous hp finite element method for convection–diffusion problems*, Computer Methods in Applied Mechanics and Engineering, (1999).

[6] Tan Bui-Thanh, Lucas C. Wilcox, Carsten Burstedde, and Omar Ghattas, *A discontinuous galerkin method for electromagnetic wave propagation on h-non-conforming adapted meshes*, in preparation, (2011).

[7] Claudio Canuto, M. Yousuff Hussaini, Alfio Quarteroni, and Thomas A. Zang, *Spectral methods*, Scientific Computation, Springer-Verlag, Berlin, 2006. Fundamentals in single domains.

[8] Bernardo Cockburn, S. Hou, and Chi-Wang Shu, *TVD Runge–Kutta local projection discontinuous Galerkin finite element method for scalar conservation laws IV: The multidimensional case*, Mathematics of Computation, 54 (1990), pp. 545–581.

[9] Bernardo Cockburn, George E. Karniadakis, and Chi-Wang Shu, *Discontinuous Galerkin Methods: Theory, Computation and Applications*, Lecture Notes in Computational Science and Engineering, Vol. 11, Springer Verlag, Berlin, Heidelberg, New York, 2000.

[10] Bernardo Cockburn and Chi-Wang Shu, *The Runge–Kutta discontinuous Galerkin method for conservation laws V*, Journal of Computational Physics, (1998), pp. 199–224.

[11] Jan S. Hesthaven, Sigal Gottlieb, and David Gottlieb, *Spectral Methods for Time-Dependent Problems*, no. 21 in Cambridge Monographs on Applied and Computational Mathematics, Cambridge University Press, January 2007.

[12] Jan S. Hesthaven and Timothy Warburton, *Nodal high-order methods on unstructured grids. I. Time-domain solution of Maxwell's equations*, Journal of Computational Physics, 181 (2002), pp. 186–221.

[13] Jan S. Hesthaven and Timothy Warburton, *Nodal Discontinuous Galerkin Methods: Algorithms, Analysis, and Applications*, vol. 54 of Texts in Applied Mathematics, Springer, 2008.

[14] David A. Kopriva, *A conservative staggered-grid chebyshev multidomain method for compressible flows. II. a semi-structured method*, Journal of Computational Physics, 128 (1996), pp. 475–488.

[15] ———, *Metric identities and the discontinuous spectral element method on curvilinear meshes*, Journal of Scientific Computing, 26 (2006), pp. 301–327.

[16] ———, *Implementing Spectral Methods for Partial Differential Equations*, Springer, 2009.

[17] David A. Kopriva and Gregor Gassner, *On the quadrature and weak form choices in collocation type discontinuous Galerkin spectral element methods*, Journal of Scientific Computing, 44 (2010), pp. 136–155.

[18] David A. Kopriva, Stephen L. Woodruff, and M. Yousuff Hussaini, *Computation of electromagnetic scattering with a non-conforming discontinuous spectral element method*, International Journal for Numerical Methods in Engineering, 53 (2002), pp. 105–122.

[19] Heinz-Otto Kreiss and Godela Scherer, *Method of lines for hyperbolic differential equations*, Siam J. Numer. Anal., 29 (1992), pp. 640–646.

[20] Peter D. Lax and Robert D. Richtmyer, *Survey of the stability of linear finite difference equations*, Communications on Pure and Applied Mathematics, 9 (1956), pp. 267–293.

[21] W. H. Reed and T. R. Hill, *Triangular mesh methods for the neutron transport equation*, Tech. Report LA-UR-73-479, Los Alamos Scientific Laboratory, 1973.

[22] William J. Rider and Robert B. Lowrie, *The use of classical Lax-Friedrichs Riemann solvers with discontinuous Galerkin methods*, Tech. Report LA-UR-01-1282, Los Alamos National Lab, 2001.

[23] Christoph Schwab, *p– and hp–finite element methods: Theory and applications in solid and fluid mechanics*, Oxford University Press, Oxford, 1998.

[24] Chun-Hao Teng, Bang-Yan Lin, Hung-Chun Chang, Hei-Chen Hsu, Chien-Nan Lin, and Ko-An Feng, *A Legendre pseudospectral penalty scheme for solving time-domain maxwell's equations*, Journal of Scientific Computing, 36 (2008), pp. 351–390.

[25] Eleuterio F. Toro, *Riemann Solvers and Numerical Methods for Fluid Dynamics*, Springer, 1999.

[26] Timothy Warburton, *Topics in numerical differential equations.* CAAM 652 lecture notes, Rice University, 2011.

[27] Lucas C. Wilcox, Georg Stadler, Carsten Burstedde, and Omar Ghattas, *A high-order discontinuous Galerkin method for wave propagation through coupled elastic-acoustic media*, Journal of Computational Physics, 229 (2010), pp. 9373–9396.